

Alma Mater Studiorum-Università di Bologna

DOTTORATO DI RICERCA IN

Meccanica e Scienze Avanzate dell'Ingegneria

Ciclo XXVII

Settore Concorsuale di afferenza: 09/C2

Settore Scientifico disciplinare: ING-IND/18

*Biomedical and industrial applications of
atmospheric pressure non-equilibrium plasmas*

Presentata da: Romolo Laurita

Coordinatore Dottorato

Relatore

Prof. Vincenzo Parenti Castelli

Prof. Vittorio Colombo

Esame finale anno 2015

“Considerate la vostra semenza
fatti non foste a viver come bruti
ma per seguir virtute e canoscenza”

Dante Alighieri, Divina Commedia, Inferno canto XXVI, 118-120

Index

1. Introduction.....	7
2. Single electrode plasma Jet.....	18
2.2. Characterization of the plasma source.....	20
2.2.1. Atmospheric pressure non-equilibrium plasma jet	20
2.2.2. Schlieren high-speed imaging	23
2.2.3. Optical emission spectroscopy.....	34
2.2.4. Temperature and heat flux measurements	44
2.3. Plasma enhanced electrospinning.....	56
2.3.1. Electrospinning process.....	58
2.3.2. Plasma treatment of polymeric solution	60

1. Introduction

My Ph.D. studies were focused on the design, realization and characterization of a non-equilibrium atmospheric pressure plasma source and the development of plasma assisted process for biomedical and industrial application. During the PhD, the plasma sources have been developed and tested in the “*Industrial applications of plasmas*” and “*Langmuir-Tesla Bio-Plasma*” laboratories at the Alma Mater Studiorum - Università di Bologna. Activities presented in this thesis have been performed into the framework of European networking projects MPNS COST Action MP1101 “Bio-Plasma - Biomedical Applications of Atmospheric Pressure Plasma Technology” and MPNS COST Action TD1208 “Electrical discharges with liquids for future applications” and PLASMAT “Plasma-assisted preparation and modification of molecular and macromolecular materials for biomedical, pharmaceutical and energy applications” (FARB2) within the activities of the Research Group for Industrial Applications of Plasmas of University of Bologna; for the activities of chapters 3 also with the contribution of AlmaPlasma S.r.l. This dissertation will be focused on the characterization of an atmospheric pressure plasma jet with an application oriented diagnostic approach and the description of processes supported by this plasma sources.

First of all, the state of the art concerning the diagnostic and applications of atmospheric pressure non-equilibrium plasmas is summarized and then results

concerning the experiment carried out using the aforementioned plasma source are presented. The plasma source investigated is a single electrode plasma jet. Schlieren images, optical emission spectra, temperature and heat flux profiles are analyzed to deeply investigate the fluid dynamic, the chemical composition and the thermal output of the plasma generated with a nanosecond-pulsed high voltage generator. The maximum temperature measured is about 45 °C and values close to the room temperature are reached 10 mm down the source outlet, ensuring the possibility to use the plasma jet for the treatment of thermosensitive materials, such as, for example, biological substrate or polymers. Electrospinning of polymeric solution allows the production of nanofibrous non-woven mats and the plasma pre-treatment of the solutions leads to the realization of defect free nanofibers. The use of the plasma jet allows the electrospinnability of a non-spinnable poly(L-lactic acid) (PLLA) solution, suitable for the production of biological scaffold for the wound dressing. 12 ml of PLLA in 100 % dichloromethane exposed to the plasma jet for 2 minutes can be electrospun without the use of any additional high boiling point toxic solvent, like dimethylformamide, that is currently added to ensure the electrospinnability of PLLA. The analysis of the acquired optical emission of the reveals the presence of OH radicals and excited N, suggesting that an important role of the reactive species produced by the plasma in the improvement of the elctrospinnability.

The results of these activities have been published on international journals:

1. M. Boselli, V. Colombo, M. Gherardi, R. Laurita, A. Liguori, P. Sanibondi, A. Stancampiano and E. Simoncelli, "Characterization of a Cold Atmospheric Pressure Plasma Jet Device Driven by Nanosecond Voltage Pulses", *IEEE Transactions on Plasma Science* (2015), DOI 10.1109/TPS.2014.2381854

2. M. Boselli, V. Colombo, E. Ghedini, M. Gherardi, R. Laurita, A. Liguori, P. Sanibondi and A. Stancampiano, "Schlieren high-speed imaging of a nanosecond pulsed atmospheric pressure non-equilibrium plasma jet", *Plasma Chemistry and Plasma Processing*, 34 (2), (2014), DOI 10.1007/s11090-014-9537-1
3. V. Colombo, D. Fabiani, M. L. Focarete, M. Gherardi, C. Gualandi, R. Laurita, M. Zaccaria, "Atmospheric Pressure Non-Equilibrium Plasma Treatment to Improve the Electrospinnability of Poly(L-lactic acid) Polymeric Solution", *Plasma Process. Polym.* 2014, DOI: 0.1002/ppap.201300141

During the PhD, a short term scientific mission (STSM) has been granted by the COST ACTION TD1208 at the *Institute of Plasma Physics, Academy of Sciences of the Czech Republic- Prague (Czech Republic)*, on the chemical analysis of the reactive species produced in water by a gas phase plasma discharges driven by nanosecond pulses.

Moreover, I took part of several different activity concerning the characterization of different atmospheric pressure plasma sources (a low power inductive coupled plasma (ICP) torch equipped with a quenching device, a nanopulsed gatling machine gun-like plasma source, a dielectric barrier discharge) and the implementation of plasma treatment of Polylactic acid electrospun mats or film. The results concerning these activities have been published on different international journals:

1. M. Boselli, V. Colombo, E. Ghedini, M. Gherardi, R. Laurita, A. Liguori, P. Sanibondi and A. Stancampiano, "High-speed and Schlieren imaging of a low power inductively coupled plasma source for potential biomedical applications", accepted for publication on *IEEE Transactions on Plasma Science -7th Triennial special issue on Images in Plasma Science*, (2014)
2. M. Boselli, V. Colombo, E. Ghedini, M. Gherardi, R. Laurita, A. Liguori, P. Sanibondi and A. Stancampiano, "High-speed multi-imaging of nanopulsed dielectric barrier discharges for potential biomedical applications", submitted to *IEEE*

Transactions on Plasma Science -7th Triennial special issue on Images in Plasma Science, (2014)

3. S. Bianconi , F. Cavrini F, V.Colombo, M.Gherardi M, R. Laurita, A. Liguori, A. Stancampiano, “iCCD imaging of a Gatling machine gun-like plasma source for biomedical and materials treatment applications”, submitted to IEEE Transactions on Plasma Science -7th Triennial special issue on Images in Plasma Science, (2014)

4. L. S. Dolci, S. D. Quiroga, M. Gherardi, R. Laurita, A. Liguori, P. Sanibondi, A. Fiorani, L. Calzà, V. Colombo, M. L. Focarete, “Carboxyl Surface Functionalization of Poly(L-lactic acid) Electrospun Nanofibers through Atmospheric Non-Thermal Plasma Affects Fibroblast Morphology”, Plasma Process. Polym. 2013, DOI: 10.1002/ppap.201300104

5. M Boselli, V Colombo, M G De Angelis, E Ghedini, M Gherardi, R Laurita, A Liguori, M Minelli, F Rotundo, P Sanibondi, A Stancampiano, “Comparing the effect of different atmospheric pressure non-equilibrium plasma sources on PLA oxygen permeability”, Journal of Physics Conference Series, vol. 406, p. 012038-012047 (2012)

During the PhD, results concerning the plasma assisted electrospinning and nanoparticles dispersion and the multi-imaging techniques for the characterization of DBD have been presented at three different international conferences with oral presentation:

1. Calzà L, Colombo V, Dolci L S, Fiorani A, Fabiani D, Focarete M L, Ghedini E, Gherardi M, Laurita R, Liguori A, Quiroga S D, Sanibondi P, Zaccaria M, “Plasma-assisted electrospinning: the many facets of a process”, oral presentation at 3rd International Conference on Electrospinning, ,San Francisco, California (US), August 2014

2. Colombo V, Fabiani D, Focarete M L, Gherardi M, Laurita R, Zaccaria M “Effect of plasma assisted nanoparticle dispersion on thermal and mechanical properties of electrospun separatorsfor lithium-ion batteries” “CIMTEC 2014- 6th Forum on new materials”, June 2014, Montecatini Terme (IT)

3. Boselli M, Colombo V, Ghedini E, Gherardi M, Laurita R, Liguori A, Sanibondi P, Stancampiano A “Multi-imaging techniques for the characterization of a nanopulsed

DBD system for biomedical applications “Plasma to plasma”, January 2013, Leiden, the Netherlands

Moreover, some results concerning diagnostic and applications of atmospheric pressure plasma have been reported in the following conference proceedings:

1. Colombo V, Favia P, Gherardi M, Gristina R, Intranuovo F, Laurita R, Liguori A, Stancampiano A, “Increasing cell viability of 3d scaffolds for tissue engineering by means of an atmospheric pressure plasma jet”, proceedings of 21th ISPC, Cairns, Australia, August 2013
2. Boselli M, Colombo V, Ghedini E, Gherardi M, Laurita R, Liguori A, Sanibondi P, Stancampiano A, “High speed imaging characterization of a Dielectric Barrier Discharge Roller plasma source”, proceedings of 21 th ISPC, Cairns, Australia, August 2013
3. Boselli M, Colombo V, Ghedini E, Gherardi M, Laurita R, Liguori A, Sanibondi P, Stancampiano A, “Characterization of a plasma jet for biomedical applications: composition, temperature, fluid dynamics and plasma structure”, proceedings of 21 th ISPC, Cairns, Australia, August 2013
4. Colombo V, Ghedini E, Gherardi M, Laurita R, Liguori A, Sanibondi P, Stancampiano A, “Parametric study on the effectiveness of treatment of polyethylene (PE) foils for pharmaceutical packaging with a large area atmospheric pressure plasma source”, proceedings of 21 ISPC, Cairns, Australia, August 2013
5. Colombo V, Ghedini E, Gherardi M, Laurita R, Liguori A, Sanibondi P, Stancampiano A, “Comparison of localized treatment effectiveness on biocompatible glass with different atmospheric pressure plasma sources”, proceedings of 21th ISPC, Cairns, Australia, August 2013
6. Alviano F, Bonsi L, Colombo V, Ghedini E, Gherardi M, Laurita R, Liguori A, Marchionni C, Marini M, Ricci F, Rossi M, Sanibondi P, Stancampiano A, Zannini C, “Study of the effect on human mesenchymal and epithelial cells of an atmospheric pressure plasma source driven by different voltage waveforms”, proceedings of 21th ISPC, Cairns, Australia, August 2013
7. Boselli M, Colombo V, Ghedini E, Gherardi M, Laurita R, Liguori A, Sanibondi P, Stancampiano A, “Study of the role of dielectric material in a dielectric barrier

discharge (DBD) plasma source for dermatological applications”, proceedings of IEEE ICSD, Bologna, Italy June 2013

8. Colombo V, Fabiani D, Focarete ML, Ghedini E, Gherardi M, Gualandi C, Laurita R, Sanibondi P, Zaccaria M. "Study of the effect of atmospheric pressure plasma treatment on electrospinnability of poly-L-lactic acid solutions: Voltage waveform effect" Solid Dielectrics (ICSD), proceedings of IEEE ICSD, Bologna, Italy June 2013

9. Colombo V, Fabiani D, Focarete ML, Ghedini E, Gherardi M, Gualandi C, Laurita R, Sanibondi P, Zaccaria M. " Plasma assisted nanoparticle dispersion in polymeric solutions for the production of electrospun lithium battery separators" Solid Dielectrics (ICSD), proceedings of IEEE ICSD, Bologna, Italy June 2013

Also, some results have been presented at international conferences:

1. Barbieri D, Boselli M, Cavrini F, Colombo V, Gherardi M, Landini M P, Laurita R, Liguori A, Sanibondi P, Stancampiano "Non-equilibrium plasma sources and processes with a focus on antibacterial applications and sterilization", keynote lecture at 14th International conference on plasma surface Engineering, Garmisch- Partenkirchen, Germany, September 2014

2. Colombo V, Fabiani D, Focarete M L, , Gherardi M, Laurita R, Zaccaria M "Nanoparticle dispersion in PEO polymeric solutions via plasma treatment for the production of electrospun lithium batteries separator" oral presentation at 3rd International Conference on Electrospinning, San Francisco, California (US), August 2014

3. Calzà L, Colombo V, Dolci L S, Fiorani A, Focarete M L, Gherardi M, Laurita R, Liguori A, Quiroga S D, Sanibondi P "Atmospheric plasma surface modification of electrospun poly(L-lactic acid): effect on mat properties and cell culturing" oral presentation at 3rd International Conference on Electrospinning, San Francisco, California (US), August 2014

4. Barbieri D, Boselli M, Cavrini F, Colombo V, Gherardi M, Landini M P, Laurita R, Liguori A, Sanibondi P, Stancampiano, Investigation of the effectiveness of a low power inductively coupled plasma source for biomedical application, invited presentation at ICPM5, Nara, Japan, May 2014

5. V. Colombo, C. Fimognari, De Gianni E, Ferruzzi L, Gherardi M, Laurita R, Liguori A, Stancampiano A, Turrini E, "Non-thermal plasma Promotes Apoptosis and cell-cycle arrest in a lymphoma cell line", oral presentation at ICPM5, Nara, Japan, May 2014

6. Cavrini F, Colombo V, Gherardi M, Laurita R, Liguori A, Polverini S, Stancampiano A, "Plasma source for the fast and continuous purification of water flows", poster presentation ICPM5, Nara, Japan, May 2014
7. Cavrini F, Colombo V, Gherardi M, Laurita R, Liguori A, Stancampiano A, "Investigation of Comparison of the growth inhibition potential of different dielectric barrier discharge operating regimes" poster presentation ICPM5, Nara, Japan, May 2014
8. Bianconi S, Cavrini F, Colombo V, Gherardi M, Laurita R, Liguori A, Stancampiano A, "Investigation of the effectiveness of a gatling machine gun-like source for biomedical and materials treatment applications" poster presentation ICPM5, Nara, Japan, May 2014
9. Boselli M, Colombo V, Gherardi M, Laurita R, Liguori A, Sanibondi P, Stancampiano A, Diagnostic of a low power inductively coupled plasma source for biomedical applications" poster presentation ICPM5, Nara, Japan, May 2014
10. Baldissara P, Colombo V, Gherardi M, Laurita R, Liguori A, Sanibondi P, Stancampiano A, " A novel plasma based teeth whitening process" poster presentation ICPM5, Nara, Japan, May 2014
11. Baldissara P, Colombo V, Gherardi M, Laurita R, Liguori A, Sanibondi P, Stancampiano A, " Plasma as a new odontoiatric tool to improve implants adhesion" poster presentation ICPM5, Nara, Japan, May 2014
12. Bloise N, Colombo V, Ferruti P, Focarete M L, Gherardi M, Gualandi C, Laurita R, Liguori A, Manfredi A, Mauro N, Ranucci E, Sampaolesi M, Visai L, " Atmospheric pressure non-equilibrium plasma for the production of composite materials" poster presentation ICPM5, Nara, Japan, May 2014
13. Anceschi G, Barbieri D, Boselli M, Cavrini F, Colombo V, Gherardi M, Landini M P, Laurita R, Liguori A, Sanibondi P, Stancampiano A, "Antimicrobial activity of a low power inductively coupled plasma at safe levels for eukaryotic cells, poster presentation ICPM5, Nara, Japan, May 2014
14. Colombo V, Fabiani D, Focarete M L, , Gherardi M, Laurita R, Zaccaria M, Plasma-assisted electrospinning: the many facets of a process, oral presentation at Workshop on Atmospheric Plasma Processes and Sources, EU COST MP1101, Bohinjjska Bistrica, Slovenia, January 2014
15. Colombo V, Fabiani D, Focarete M L, Gherardi M, Laurita R, Zaccaria M, Processes and sources for biomedical and surface treatment applications in UNIBO,

invited presentation at Workshop on Atmospheric Plasma Processes and Sources, EU COST MP1101, Bohinjka Bistrica, Slovenia, January 2014

16. Cavrini F, Colombo V, Gherardi M, Laurita R, Liguori A, Polverini S, Stancampiano A, "Plasma source for the fast and continuous purification of water flows", poster presentation at COST TD1208 Annual Meeting, Lisbon, March 2014

17. Alviano F, Bonsi L, Colombo V, Ghedini E, Gherardi M, Laurita R, Liguori A, Marchionni C, Marini M, Ricci F, Rossi M, Sanibondi P, Stancampiano A, Zannini C, "Study of the effect on human mesenchymal and epithelial cells of an atmospheric pressure plasma source driven by different voltage waveforms", poster presentation at 18th European Summer School Low Temperature Plasma Physics, October 2013

18. Colombo V, Favia P, Gherardi M, Gristina R, Intranuovo F, Laurita R, Liguori A, Stancampiano A, "Increasing cell viability of 3d scaffolds for tissue engineering by means of an atmospheric pressure plasma jet", poster presentation at 21 th ISPC, Cairns, Australia, August 2013

19. Boselli M, Colombo V, Ghedini E, Gherardi M, Laurita R, Liguori A, Sanibondi P, Stancampiano A, "High speed imaging characterization of a Dielectric Barrier Discharge Roller plasma source", poster presentation at 21th ISPC, Cairns, Australia, August 2013

20. Boselli M, Colombo V, Ghedini E, Gherardi M, Laurita R, Liguori A, Sanibondi P, Stancampiano A, "Characterization of a plasma jet for biomedical applications: composition, temperature, fluid dynamics and plasma structure", poster presentation at 21 th ISPC, Cairns, Australia, August 2013

21. Alviano F, Bonsi L, Colombo V, Ghedini E, Gherardi M, Laurita R, Liguori A, Marchionni C, Marini M, Ricci F, Rossi M, Sanibondi P, Stancampiano A, Zannini C, "Study of the effect on human mesenchymal and epithelial cells of an atmospheric pressure plasma source driven by different voltage waveforms", poster presentation at 21th ISPC, Cairns, Australia, August 2013

22. Colombo V, Ghedini E, Gherardi M, Laurita R, Liguori A, Sanibondi P, Stancampiano A, "Comparison of localized treatment effectiveness on biocompatible glass with different atmospheric pressure plasma sources", poster presentation at 21th ISPC, Cairns, Australia, August 2013

23. Colombo V, Fabiani D, Focarete M L, Ghedini E, Gherardi M, Laurita R, Sanibondi P, Zaccaria, "Effect of atmospheric pressure non-equilibrium plasma treatment on poly-L-lactic acid electrospinnability", poster presentation at ISPC21, Cairns, Australia, 4-9 August 2013

24. Colombo V, Fabiani D, Focarete M L, Ghedini E, Gherardi M, Laurita R, Sanibondi P, Zaccaria, "Study of the effect of atmospheric pressure plasma treatment on electrospinnability of poly-L-lactic acid solutions: voltage waveform effect", poster presentation at ISPC21, Cairns, Australia, 4-9 August 2013
25. Colombo V, Ghedini E, Gherardi M, Laurita R, Liguori A, Sanibondi P, Stancampiano A, "Parametric study on the effectiveness of treatment of polyethylene (PE) foils for pharmaceutical packaging with a large area atmospheric pressure plasma source", poster presentation at PPPS 2013, San Francisco, USA, 16-21 June 2013
26. Boselli M, Colombo V, Ghedini E, Gherardi M, Laurita R, Liguori A, Rotundo F, Sanibondi P, Stancampiano A, "Multi-imaging techniques for the characterization of a nanopulsed dbd system for biomedical applications"
27. Colombo V, Fabiani D, Focarete M L, Ghedini E, Gherardi M, Laurita R, Sanibondi P, Zaccaria M, "Effect of atmospheric pressure non-equilibrium plasma treatment on poly-L-lactic acid electrospinnability", poster presentation at NanotechItaly 2012, Venice, Italy, 21-23 November 2012
28. Alessandri M, Calzà L, Colombo V, Dolci L S, Fiorani A, Focarete M L, Ghedini E, Gherardi M, Laurita R, Liguori A, Sanibondi P, Zucchelli A, "Atmospheric plasma surface modification of electrospun poly(L-lactic acid): effect on mat properties and cell culturing", oral presentation at BIOINTERFACE 2012, University College, Dublin, Ireland, 23-25 October 2012
29. Boselli M, Colombo V, Ghedini E, Gherardi M, Laurita R, Sanibondi P, "Optimization oriented characterization of a dual gas plasma needle device for biomedical applications: effluent composition, thermal output and fluid dynamics", poster presentation at GRC - Plasma Processing Science and Societal Grand Challenges, Bryant University, Smithfield, USA, 22-27 July 2012
30. Boselli M, Colombo V, Ghedini E, Gherardi M, Laurita R, Sanibondi P, "Optimization oriented characterization of a dual gas plasma needle device for biomedical applications: effluent composition, thermal output and fluid dynamics", oral presentation at GRS - Plasmas in Biology and Medicine, Plasma Processing and Plasma Analysis and Diagnostics, Bryant University, Smithfield, USA, 22-27 July 2012
31. Boselli M, Colombo V, Ghedini E, Gherardi M, Laurita R, Rotundo F, Sanibondi P, "Multi-imaging techniques for the characterization of a nanopulsed DBD system for biomedical applications", oral presentation at GRS - Plasmas in Biology and Medicine, Plasma Processing and Plasma Analysis and Diagnostics, Bryant University, Smithfield, USA, 22-27 July 2012

32. Boselli M, Colombo V, Ghedini E, Gherardi M, Laurita R, Liguori A, Rotundo, Sanibondi P, Stancampiano A, "Fluid-dynamic characterization of atmospheric pressure non-equilibrium plasma sources for biomedical applications", poster presentation at ICOPS 2012, Edinburgh, Scotland, 8-12 July 2012
33. Boselli M, Colombo V, De Angelis M G, Ghedini E, Gherardi M, Laurita R, Minelli M, Rotundo F, Sanibondi P, Stancampiano A, "Comparing the effects of different atmospheric pressure non-equilibrium plasma sources on PLA oxygen permeability", poster presentation at ICOPS 2012, Edinburgh, Scotland, 8-12 July 2012
34. Boselli M, Colombo V, Ghedini E, Gherardi M, Laurita R, Liguori A, Rotundo F, Sanibondi P, Stancampiano A, "Multi-imaging techniques for the characterization of a nanopulsed DBD system for biomedical applications", oral presentation at HTPP12, Bologna, Italia, 24-29 June 2012
35. Boselli M, Colombo V, Ghedini E, Gherardi M, Laurita R, Liguori A, Sanibondi P, Stancampiano A, "Fluid-dynamic characterization of atmospheric pressure non-equilibrium plasma sources for biomedical applications", poster presentation at HTPP12, Bologna, Italia, 24-29 June 2012
36. Boselli M, Colombo V, De Angelis M G, Ghedini E, Gherardi M, Laurita R, Minelli M, Sanibondi P, Stancampiano A, "Comparing the effects of different atmospheric pressure non-equilibrium plasma sources on PLA oxygen permeability", poster presentation at HTPP12, Bologna, Italia, 24-29 June 2012
37. Boselli M, Colombo V, Ghedini E, Gherardi M, Laurita R, Liguori A, Sanibondi P, Stancampiano A, "Transition from non-uniform to uniform discharge in nanosecond pulsed FE-DBD and linear corona non-equilibrium plasmas", poster presentation at HTPP12, Bologna, Italia, 24-29 June 2012
38. Boselli M, Colombo V, Ghedini E, Gherardi M, Laurita R, Liguori A, Sanibondi P, Stancampiano A, "Effluent composition, thermal output and fluid-dynamics of a dual gas plasma needle device for biomedical applications: Part II", poster presentation at HTPP12, Bologna, Italia, 24-29 June 2012
39. Boselli M, Colombo V, Ghedini E, Gherardi M, Laurita R, Liguori A, Sanibondi P, Stancampiano A, "Effluent composition, thermal output and fluid-dynamics of a dual gas plasma needle device for biomedical applications: Part I", poster presentation at HTPP12, Bologna, Italia, 24-29 June 2012
40. Boselli M, Colombo V, Ghedini E, Gherardi M, Laurita R, Liguori A, Rotundo F, Sanibondi P, Stancampiano A, "Multi-imaging techniques for the characterization of a

nanopulsed DBD system for biomedical applications”, oral presentation at 5P Plasma Processes: Past. Present and Perspectives, Bari, Italia, 21-23 June 2012

41. Boselli M, Colombo V, Ghedini E, Gherardi M, Laurita R, Liguori A, Rotundo F, Sanibondi P, Stancampiano A, “Effluent composition, thermal output and fluid-dynamics of a dual gas plasma needle device for biomedical applications: Part I”, poster presentation at ICPM4, Orléans, France, 17-21 June 2012

42. Boselli M, Colombo V, Ghedini E, Gherardi M, Laurita R, Liguori A, Rotundo F, Sanibondi P, Stancampiano A, “Effluent composition, thermal output and fluid-dynamics of a dual gas plasma needle device for biomedical applications: Part II”, poster presentation at ICPM4, Orléans, France, 17-21 June 2012

43. Boselli M, Colombo V, Ghedini E, Gherardi M, Laurita R, Liguori A, Rotundo F, Sanibondi P, Stancampiano A, “Transition from non-uniform to uniform discharge in nanosecond pulsed FE-DBD and linear corona non-equilibrium plasmas”, poster presentation at ICPM4, Orléans, France, 17-21 June 2012

2. Single electrode plasma Jet

In recent years, atmospheric pressure non-equilibrium plasmas have been proven to be viable tools for decontamination and sterilization of surfaces and living tissues [1-5]; currently, exploration of the feasibility of plasma aided medical therapies, such as blood coagulation, chronic wound remediation and cancer treatment, is at the forefront of research in plasma applications [6-18]. While this exciting field promises breakthrough discoveries and revolutionary therapies, the complexity of plasma interaction with biological materials and the stiff requisites imposed by biomedical treatments put a premium on diagnostics as a mean to investigate process feasibility and to develop plasma sources tailored for specific applications; moreover, this multidisciplinary task requires integrated approaches relying not only on the effectiveness of the treatments, but also on the characterization of the plasma sources, in order to promote an effective multi-step optimization of the process. Consequently, the scientific community has dedicated large efforts to identify the most suitable diagnostic techniques to characterize different plasma sources for biomedical applications [19-25].

The macroscopic aspect of the non-thermal plasma discharge can be characterized by means of low speed imaging, [26-27], but this diagnostic has a limited efficacy for the description of fluid-dynamic phenomena. A qualitative and very effective study of the fluid-dynamic behavior of a jet can be performed conducted by Schlieren imaging. Schlieren photography has already been used to investigate turbulence in the plasma generated by different plasma jet sources: as an example, Bradley *et al* used Schlieren

photography to investigate laminar and turbulent flows of a microjet generated in He on a polystyrene surface and also to determine the length of laminar and turbulent flow regions [28].

In order to identify reactive species produced in non-thermal plasmas, optical emission spectroscopy (OES) is widely adopted in the characterization of plasma sources for biomedical applications [24, 25]. Some of these species have strong and well-documented valuable effects on cells and tissues, such as microbial decontamination [29], acceleration of wound healing [30] and blood coagulation [31]; on the other hand, some reactive species may cause cytotoxic effects or lead to cell and tissue damage [32], raising the need for their monitoring and control.

Furthermore the estimation of the plasma temperature and power transfer from the plasma is important for the diagnostic of the plasma source for direct medical applications, because these parameters represent a risk factor in the direct interaction with biological substrates and living tissues [19]. Among different approaches, fiber optic sensor seems to be the best choice to obtain accurate gas temperature measurements since it has an acceptably low response time without being susceptible to interference from high voltages and high frequency electromagnetic fields typically encountered in the plasma environment [33, 34]. The same sensors can also be used to measure the heat flux of the jet as proposed in [19].

2.2. Characterization of the plasma source

In this chapter the diagnostic of a single electrode plasma jet is presented. The plasma source investigated is a single electrode plasma jet. High speed Schlieren images, optical emission spectra, temperature and heat flux profiles are analysed to deeply investigate the fluid dynamic, the chemical composition and the thermal output of the plasma plume.

2.2.1. Atmospheric pressure non-equilibrium plasma jet

The plasma source used in this work is a single electrode plasma jet [35] developed in our laboratory and previously reported in [36]; a schematic of the source is presented in Fig. 2.1. This plasma source can be operated with two different gas supplies at the same time. Two separate inlets for gases are located in the case, made in DELRIN, in order to introduce a primary gas sustaining the plasma (Ar, He, Air) and to separately inject a secondary gas (O_2 , N_2 , gas-phase monomer). The primary gas is injected through a 12-hole (0.3 mm diameter) diffuser that ensures an uniform and laminar distribution of the primary gas flow along the electrode, while the secondary gas can be introduced through twelve 0.3 mm holes, tilted with respect to the plasma jet axis. The high voltage electrode is a stainless steel sharpened metallic needle with a diameter of 0.3 mm and 19.5 mm long; the electrode protrudes from a quartz capillary (outer diameter of 1 mm) by 3 mm. The external orifice of the plasma source has a diameter of 1 mm. The plasma source can be driven by different high voltage generators.

The plasma source is driven by a commercial pulse generator (FID GmbH - FPG 20-1NMK) producing high voltage pulses with a slew rate of few kV/ns, a peak voltage (PV) of 7-20 kV into a 100-200 Ω load impedance and a maximum pulse repetition frequency (PRF) of 1000 Hz. A typical voltage waveforms applied to the plasma source during operation is presented in Fig. 2.2. The jet can be also driven by a HV Amplifier (Trek model 30/20-H-CE, ± 30 kV, 20 mA) connected to a function generator (Stanford Research model DS335, 3 MHz) operating with a microsecond rise time and several waveforms such as sinusoidal, triangular, square and sawtooth. Fig. 2.3 shows the differences between jet generated using Ar or He as primary gas at the same operating conditions.

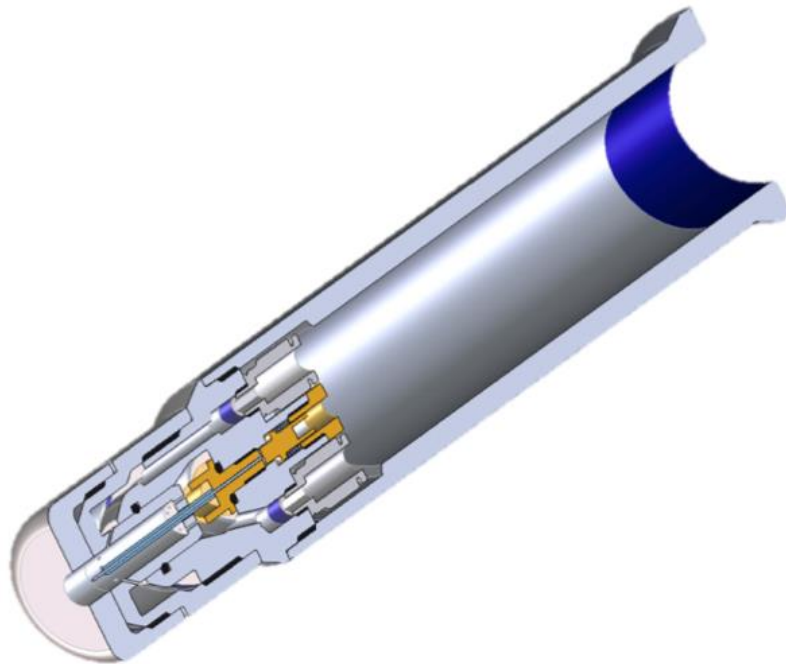


Fig. 2.1 Three dimensional cross-section representation of the plasma jet source [36]

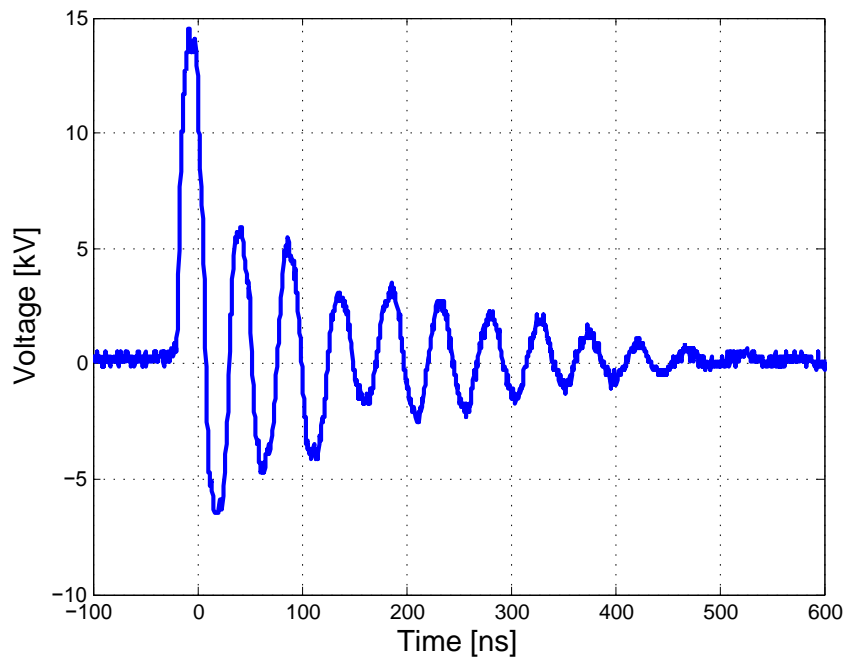


Fig.2.2 Typical voltage waveform applied to the plasma source [36]

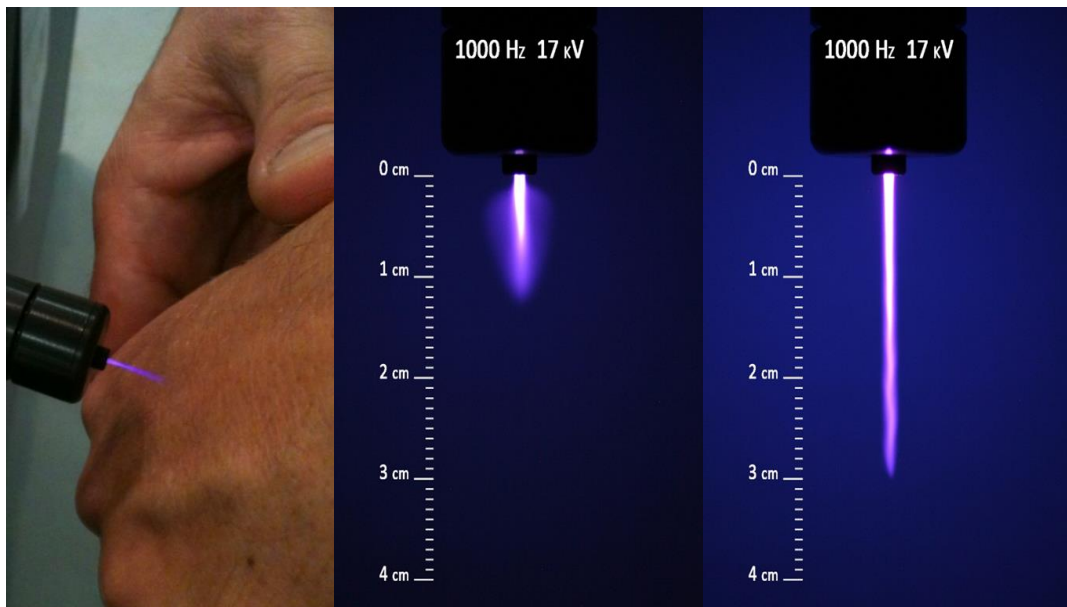


Fig. 2.3 Low speed imaging of the plasma jet treating a hand (left); picture of the plasma jet operated in Ar at flow rate 3 slpm, PRF 1000 Hz and PV 17 kV (centre); picture of the plasma jet operated in He at flow rate 3 slpm, PRF 1000 Hz and PV 17 kV (right) [36]

2.2.2 Schlieren high-speed imaging

The fluid-dynamic characterization by means of Schlieren high-speed imaging of the effluent region of the single electrode plasma jet driven by nanosecond pulsed high voltage generator is presented. This research has been performed in close collaboration with Marco Boselli and the results presented in the following pages have been published in [37]. Time evolution of fluctuations generated in a free flow regime was investigated. The primary gas is helium (He) with a mass flow rate (Q) of 1, 3 and 5 slpm, while secondary gas was not employed. The Reynolds number of the He flow without plasma ignition is calculated equal to 170, 500 and 840, respectively.

2.2.2.1 High-speed Schlieren imaging setup

The behaviour of the plasma jet was investigated through a Schlieren imaging setup in a Z configuration (Fig. 2.4.). The diagnostic setup consists of a 450 W Ozone Free Xenon Lamp (Newport-Oriel 66355 Simplicity Arc Source), a slit and an iris diaphragm, two parabolic mirrors with a focal length of 1 m, a knife edge positioned vertically and a high-speed camera [37].

The plasma jet has been positioned in the middle of the optical path between the parabolic mirrors, with the gas flow and plasma plume direction having a vertically downward direction. A high-speed camera (Memrecam K3R- NAC Image Technology), with of 4000 fps and 1/50000 s shutter time, was used to visualize the turbulent region of the plasma jet operated in free flow. Moreover, a second high-speed camera (Memrecam GX-3- NAC Image Technology), operating at 4000 fps and 1/200000 s

shutter time was used to study the plasma jet behaviour when impinging plasma on different substrates. Since the duration of the high-voltage pulse driving the plasma source is less than 500 ns and the time span for each high-speed camera frame is 0.25 ms, during the voltage pulse only one frame is recorded, which has been labelled with $t = 0$ ms.

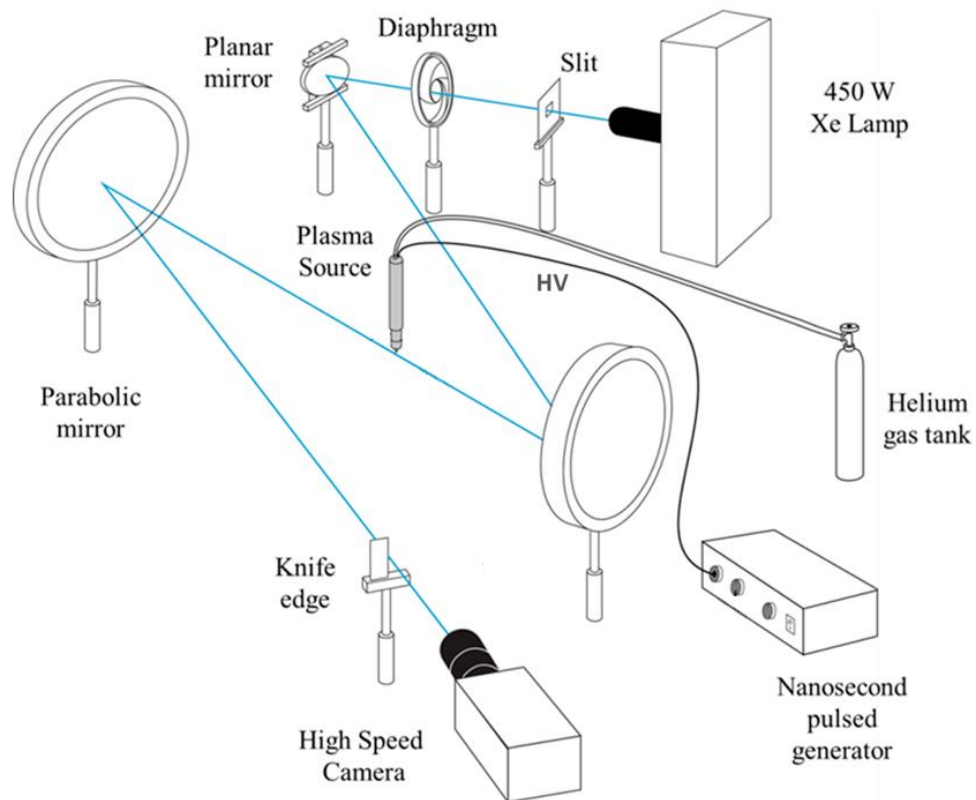


Fig. 2.4 Experimental setup for high-speed Schlieren imaging [38]

The plasma jet outflow has been investigated for different substrates and for the case with no substrate (free flow jet). Three different substrates have been tested: a grounded metallic substrate made of anodized aluminium, the same grounded metallic substrate covered with a dielectric layer (PVC tape 0,15 mm thickness) and a polystyrene Petri dish (DxH 1x4 cm). All the substrates were posed at 1.8 cm from the outlet of the plasma source. The substrate characteristics have negligible effects on the voltage waveform applied to the electrode [37].

2.2.2.2 Free flow jet

In order to describe an overall phenomenon, a set of different low speed images of the plasma jet taken with conventional camera (Fig. 2.5). A flow rate (Q) increase from 1 to 3 He slpm induced a length increase of the plasma plume, whereas a further increase up to 5 slpm resulted in a turbulent behavior of the plume, due to the increased shear force between the high velocity jet and the surrounding air. If the plasma jet is operated with a flow rate of 1 and 3 slpm of He, corresponding to a Reynolds number of 170 and 500, respectively. When the flow rate is increased to 5 slpm, the Reynolds number falls inside a transition range (between 500 and 1000) in which the jet becomes unstable at a certain distance from the nozzle. . According to [39], a jet is completely laminar for Reynolds numbers below 500.

A direct comparison between conventional and Schlieren frames of a plasma jet in the same operating conditions is presented in Fig. 2.6. The complete propagation of plasma jet in the surrounding air, the effective length of the laminar region and the

structure of the eddies of the turbulent zone can be observed in Schlieren frames, whereas they cannot be seen in conventional photography.

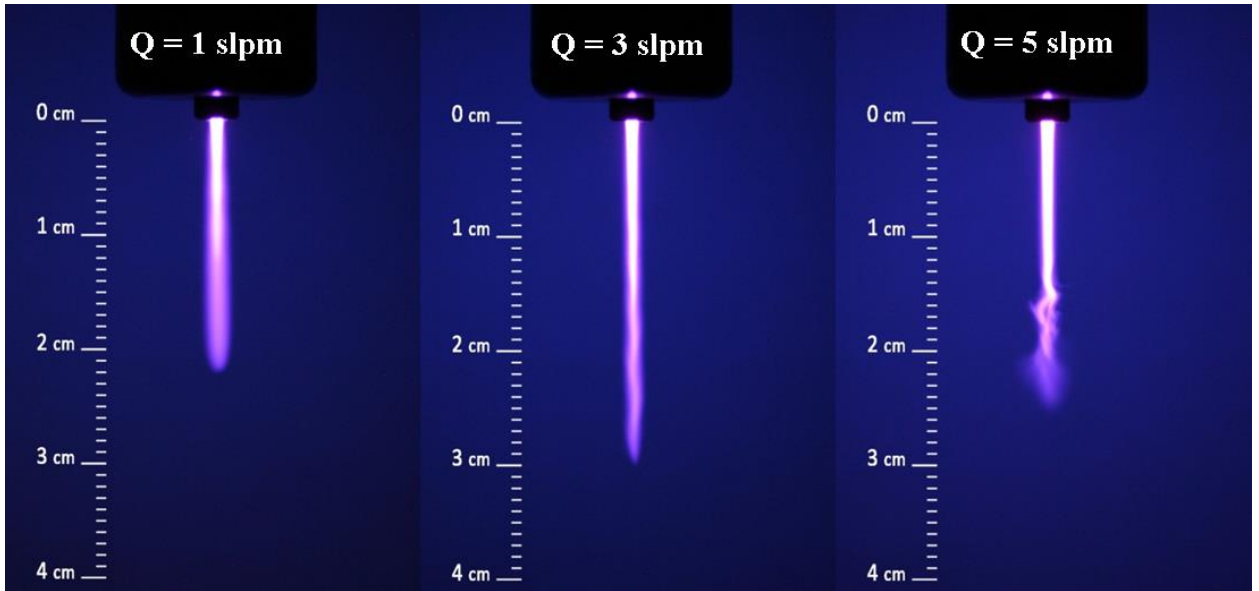


Fig. 2.5 Low speed imaging of plasma jets operated with PRF = 1 kHz, PV = 17 kV and different He mass flow rate [37]

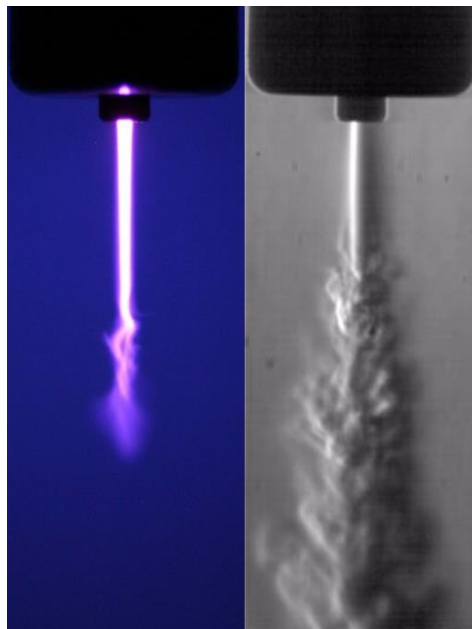


Fig. 2.7 Conventional low speed imaging (left) and high speed Schlieren imaging (right) of a He plasma jet with PV = 17 kV, PRF = 1 kHz and mass flow rate = 5 slpm [37]

If the Schlieren images were recorded without any plasma ignition (Fig. 2.8a) a transition from laminar to turbulent flow was observed when the mass flow rate was increased from 3 slpm to 5 slpm. In particular, the 3 slpm case showed a completely laminar regime, whereas in the 5 slpm case the effluent flow is characterized by a first laminar zone 1.5 cm long followed by an unstable zone with many visible eddies, due to the turbulent mixing of He with the surrounding air.

When plasma is ignited fluid-dynamic instabilities occurred also for 3 slpm, while for the 5 slpm case a decrease of the laminar region length from 1.5 cm to 0.5 cm was evinced, as shown in Fig. 2.8b.

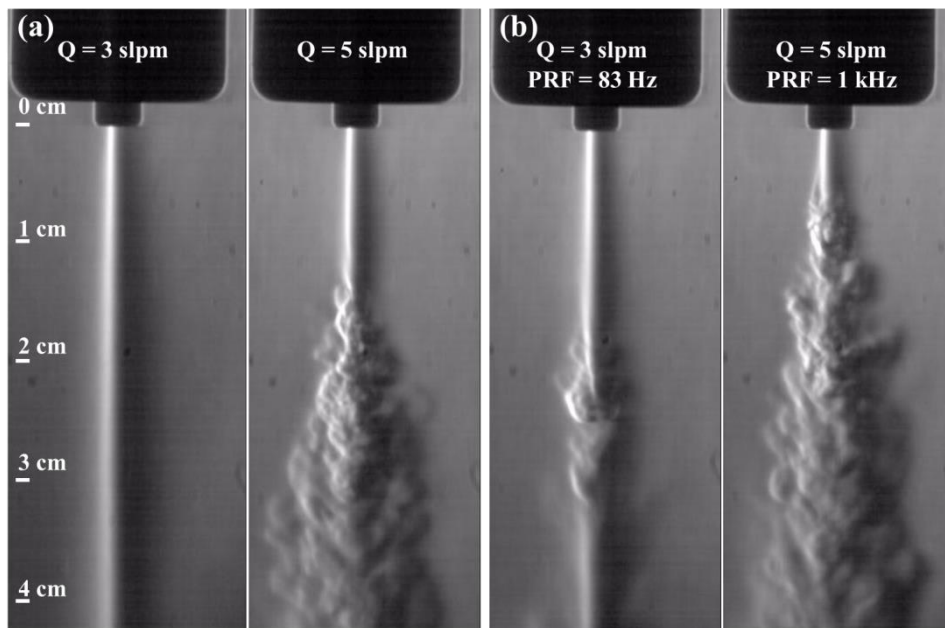


Fig. 2.8 Schlieren imaging of effluent fluid-dynamics of different mass flow rate without plasma generation (a) and with plasma ignition ($PV = 20$ kV) in two different operative conditions (b) [37]

In Fig. 2.9, frames for the case of the plasma jet operated with $PV = 20$ kV, $PRF = 83.3$ Hz and a He mass flow rate of 3 slpm are presented, in order to show the temporal evolution of the plasma jet fluid-dynamics in the time span of two voltage

pulses. At 0.5 ms before the voltage pulse, the jet is mostly laminar. After 1.5 ms from the voltage pulse, a turbulent front was observed which propagates in the downstream region. The observed turbulent front propagation is similar for each voltage pulse: in the frame acquired at $t = 14.5$ ms, which correspond to a delay of 2.5 ms after the second voltage pulse, the fluid-dynamic structure of the plasma jet was similar to that of the frame at 2.5 ms, with the formation of a turbulent front 1.5 cm downstream the nozzle. The propagation velocity of the turbulent front along the laminar region was estimated, by analyzing the high-speed Schlieren acquisitions, to be about 60 m/s, which is close to the calculated mean gas velocity.

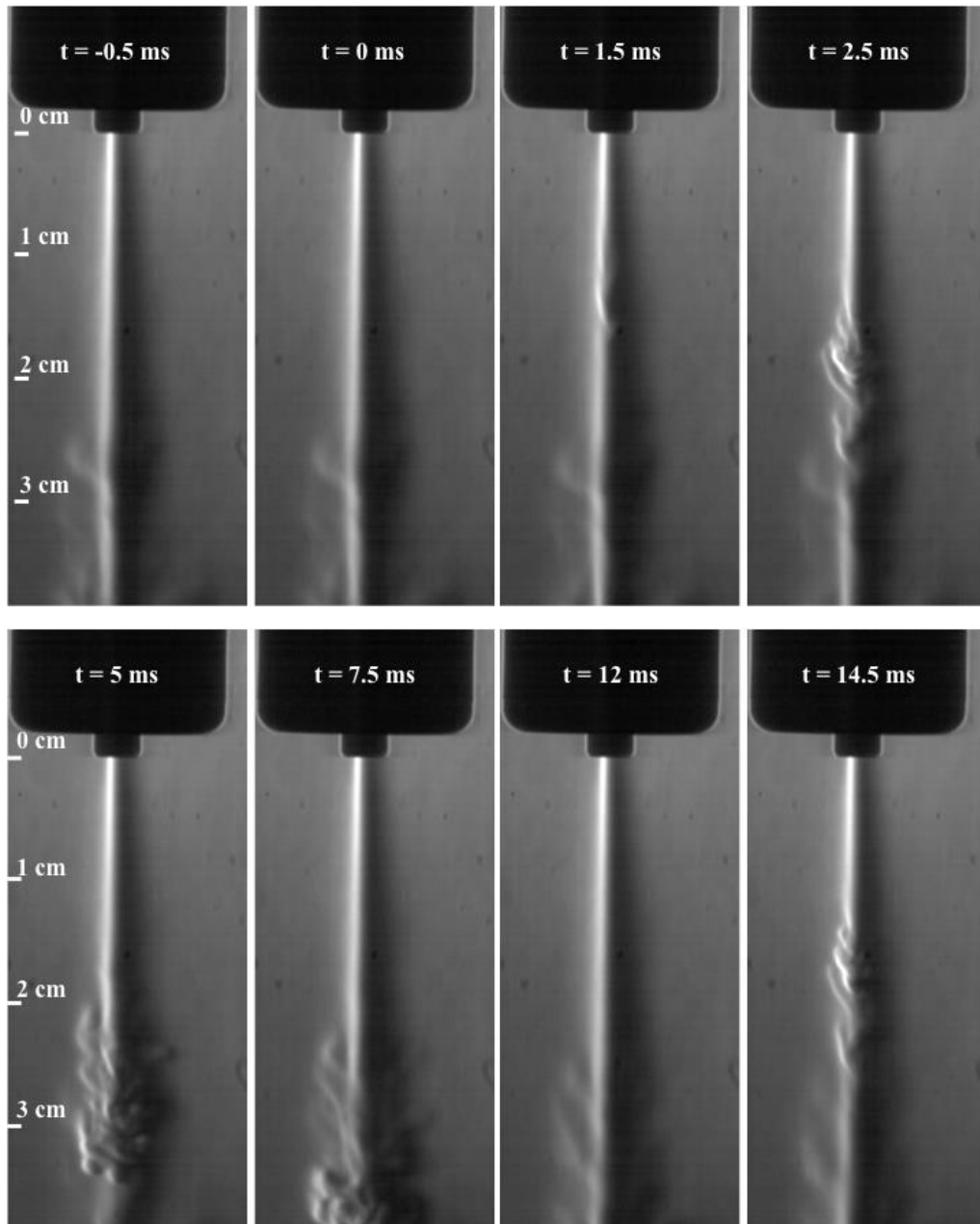


Fig. 2.9 Schlieren imaging of the plasma jet evolution between two voltage pulses, at $t = 0$ ms and $t = 12$ ms. $PV = 20$ kV, $PRF = 83.3$ Hz and He mass flow rate = 3 slpm [37]

In Fig. 2. 10, Schlieren images of the plasma jet generated with $PV = 20$ kV, $PRF = 125$ Hz and He mass flow rate = 5 slpm are presented, the fluid-dynamic structure 0.25 ms before the voltage pulse ($t = -0.25$ ms) was characterized by a laminar zone

propagating 2 cm downstream the nozzle, followed by a turbulent zone. During voltage pulse (starting at $t = 0$ ms), the formation of a turbulent front inside the laminar region was observed. The propagation of the turbulent front was tracked in the frame sequence from $t = 0.25$ ms to $t = 4$ ms.

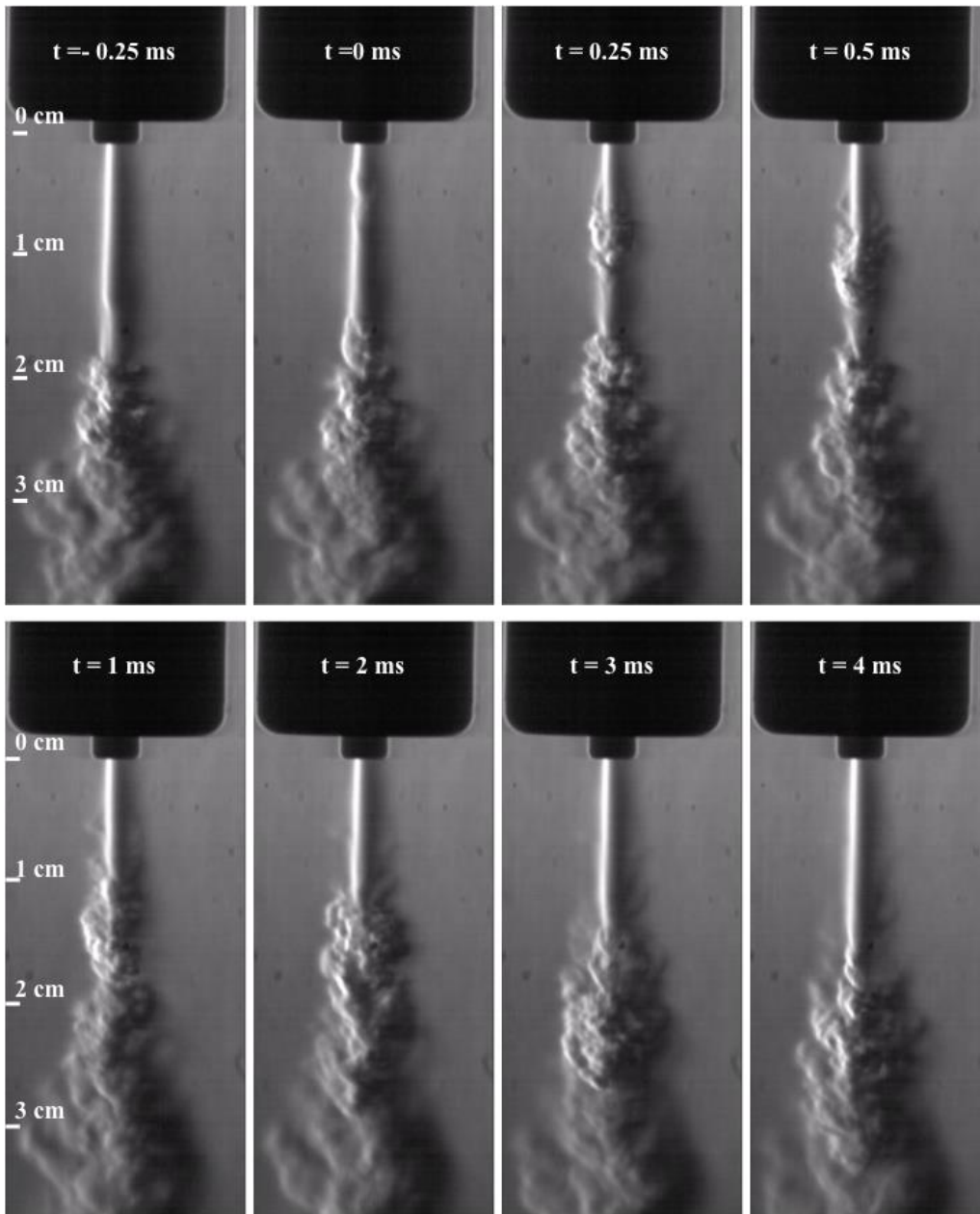


Fig. 2.10 Schlieren imaging of the plasma jet fluid-dynamics during a voltage pulse, starting at $t = 0$ ms. PV = 20 kV, PRF = 125 Hz, and He mass flow rate = 5 slpm [37]

If the PRF was increase up to 1000 Hz, the time required for the turbulent front to travel along the laminar region (around 1 ms) becomes comparable with the period between voltage pulses (1 ms); in this case, no turbulent front propagation can be observed between voltage pulses: as can be seen in Fig. 2.11, the Schlieren acquisitions of the jet before ($t = -0.25$ ms) and after ($t = 0.25$ ms) the voltage pulse, which occurs at $t = 0$ ms, are very similar to one another. The effects of the peak voltage on the plasma jet evolution at high repetition frequency are highlighted in figures 2.11a and 2.11b. The increase of the peak voltage from 14 kV (Fig. 2.11a) to 20 kV (Fig. 2.11b) induced a shortening of the laminar region from 3 cm to 1.5 cm. Comparing different time frames in the same operating conditions, no relevant differences for the laminar region length were notable in the plasma jet fluid-dynamic structure before and after the pulse. From the comparison between Fig. 2.8a and Fig. 2.11, it can be seen that plasma ignition with PRF at 1000 Hz induces the onset of a turbulent behavior in the tail of the jet.

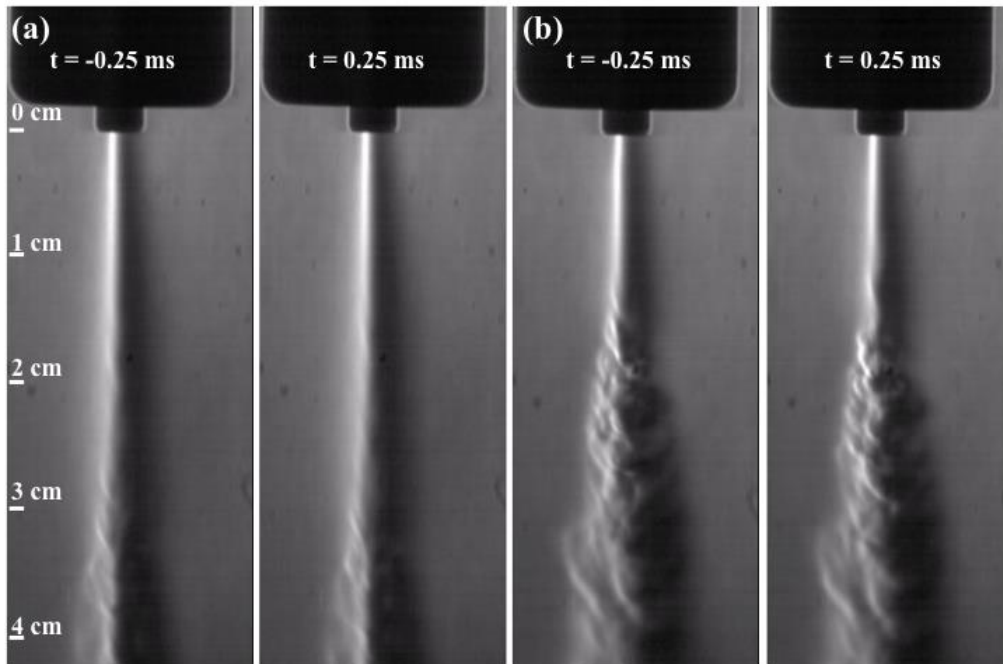


Fig. 2.11 Schlieren imaging of the plasma jet operated with PV = 14 kV (a) and 20 kV (b). PRF= 1 kHz, He mass flow rate = 3 slpm [37]

The high speed Schlieren images presented have shown that plasma ignition induced the formation of a turbulent front which propagated along the jet; moreover, if the period between subsequent voltage pulses was comparable with time required for the turbulent front to propagate along the laminar region of the jet (about 1 ms), the onset of turbulence induced the reduction of the jet laminar region [37]. Similar results concerning the reduction of the laminar region length due to plasma ignition has been already observed for other plasma jets driven by AC voltage waveforms and nanosecond pulses [28, 40].

Gas heating, local pressure increase, variation of transport properties of gas or momentum transfer between ions and neutrals are supposed to be mechanisms responsible for the formation of a turbulent front in correspondence of the high-

voltage pulse, but this phenomenon is still poorly understood. Gas heating during the voltage pulse can induce the reduction of gas density, which in turn results in a localized increase of gas velocity; a pressure peak can also take place near the powered electrode during the voltage pulse as a consequence of local ionization, with a subsequent increase of jet velocity; also, the variation of the transport properties of gas (especially viscosity) in presence of ionized species during the pulse can result in a gradient of gas velocity and in the formation of a turbulent front; finally, when the structure of the plasma jet is characterized by plasma bullets, which are travelling with a velocity of several km/s [18], turbulence onset can be linked to momentum transfer between ions and neutrals.

Plasma ignition causes fluid-dynamic instabilities that are moving in the direction of the jet flow and are correlated with the high-voltage pulses: for low pulse repetition frequency (<125 Hz) it is possible to track the movement of the turbulent front between two voltage pulses, whereas for higher pulse repetition frequency (1000 Hz) the flow is completely characterized by turbulent eddies in the effluent region without relevant changes between the voltage pulses. Plasma ignition causes fluid-dynamic instabilities moving in the direction of the jet flow and correlated with the high-voltage pulses: for low pulse repetition frequency (<125 Hz), the movement of the turbulent front between two voltage pulses can be tracked, whereas for higher pulse repetition frequency (1000 Hz) the flow is completely characterized by turbulent eddies in the effluent region, without relevant changes between subsequent voltage pulses [37].

2.2.3 Optical emission spectroscopy

Effluent composition of the plasma jet driven by high-voltage pulses with nanosecond rise time is characterized by means of spatially resolved optical emission spectroscopy; spectra in the ultraviolet, visible and near-infrared regions are reported in this chapter, in order to highlight the behaviour of several bioactive molecules and radicals (e.g. NO, OH, O).

2.2.3.1 Optical emission spectroscopy setup

Spatially resolved optical emission spectra in the ultraviolet (UV), visible (VIS) and near infrared (NIR) regions were collected perpendicular to the plasma jet and along its axis using a 500 mm spectrometer (Acton SP2500i, Princeton Instruments) synchronized with an iCCD camera (PIMAX3, Princeton Instruments), while voltage signal was recorded by means of an oscilloscope (Tektronix DP4040), as shown in Fig. 2.12. Measurements have been performed using a lens with 30 mm focal length, slit width set at 20 μm and exposure time at 20 μs . Spectra were collected in the region extending from the source outlet to 15 mm downstream, with a 0.1 mm spatial resolution and a 0.17 nm spectral resolution. A chromatic scale is adopted to refer to emission intensity of all spatially resolved spectra [38].

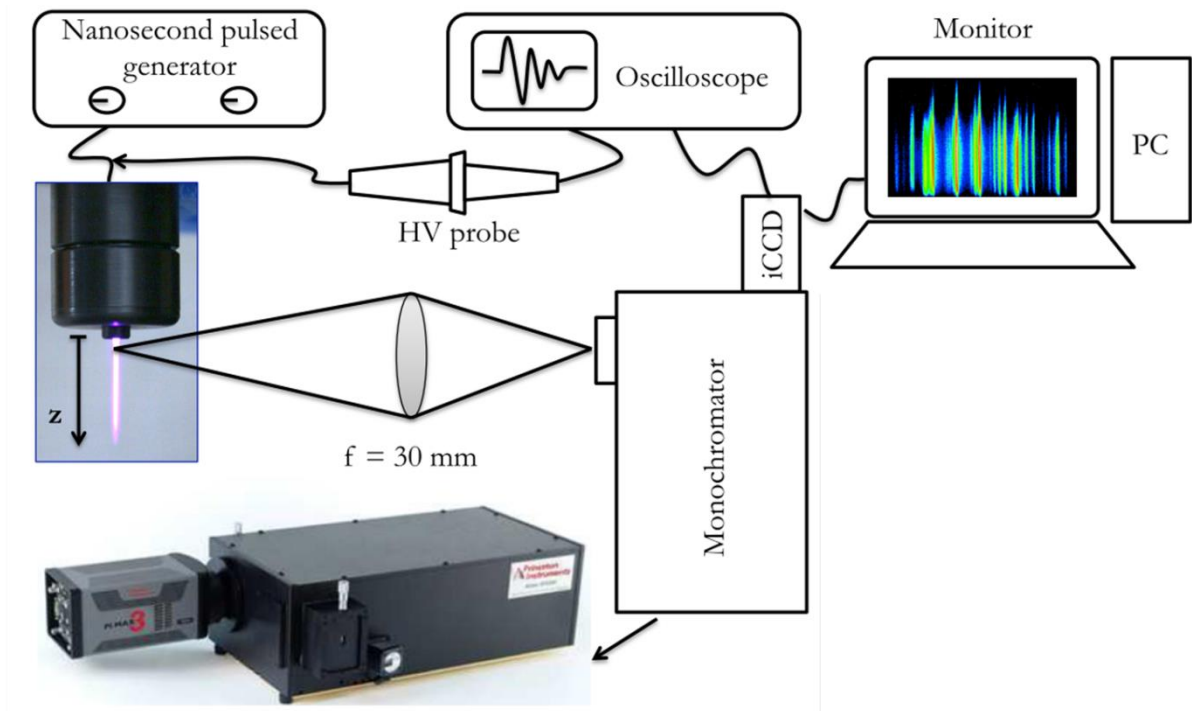


Fig. 2.12: Schematic of the OES setup

2.2.3.2 OES measurements in UV-VIS range

Optical emission spectra in the UV-VIS region from 250 up to 500 nm measured at different axial positions of the plasma jet at 330 Hz, 20 kV and an He primary gas flow rate of 5 slpm are shown in Fig. 4b, while a 0-dimensional spectrum for the same operative conditions at a fixed position is presented in Fig. 2.13a. Lines of nitrogen emission were measured in the near UV (NUV) region between 300 and 400 nm, while OH radicals in the UVB region around 307 nm were registered. A faint emission in the UVC region due to NO radicals was also observed.

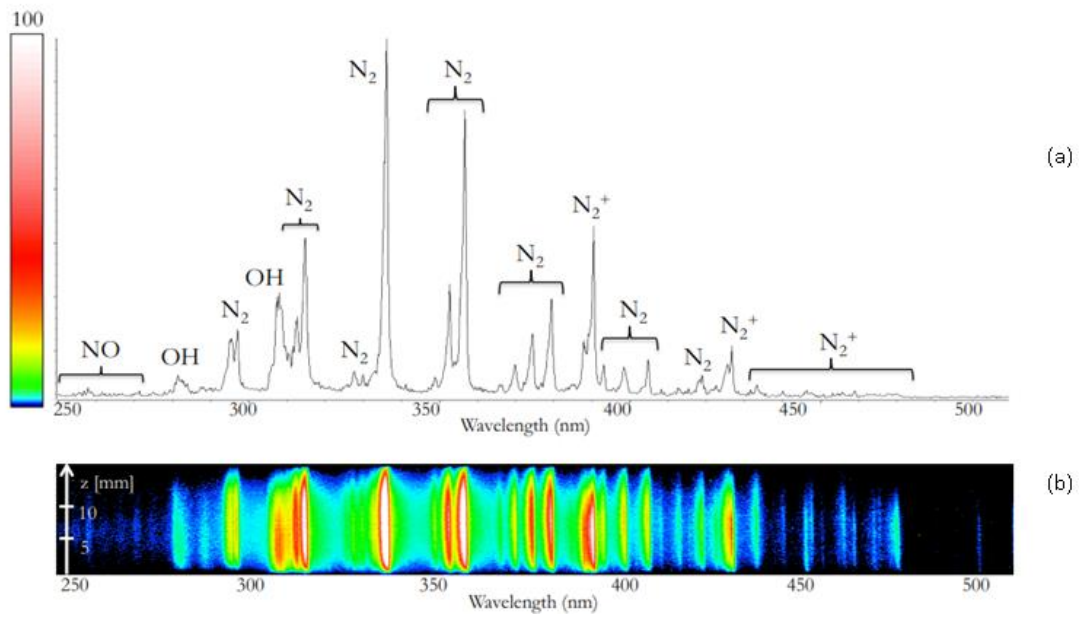


Fig. 2.13 Optical emission spectra of the plasma jet, operative conditions: primary gas He 5 slpm, PRF 330 Hz, PV 20 kV. Zero dimensional spectrum of the plasma jet at a distance 5 mm from the source outlet (a); spatially resolved spectra (b)

The effect of the primary gas on the spectra emitted by the plasma jet is highlighted in Fig. 2.14, where results for He and Ar are compared; for both configurations pulse repetition frequency was set at 330 Hz, peak voltage at 16 kV and primary gas flow rate was 1 slpm. With Ar as primary gas higher emission intensity of OH species was observed, while for a He plasma jet a stronger N_2 emission was observed.

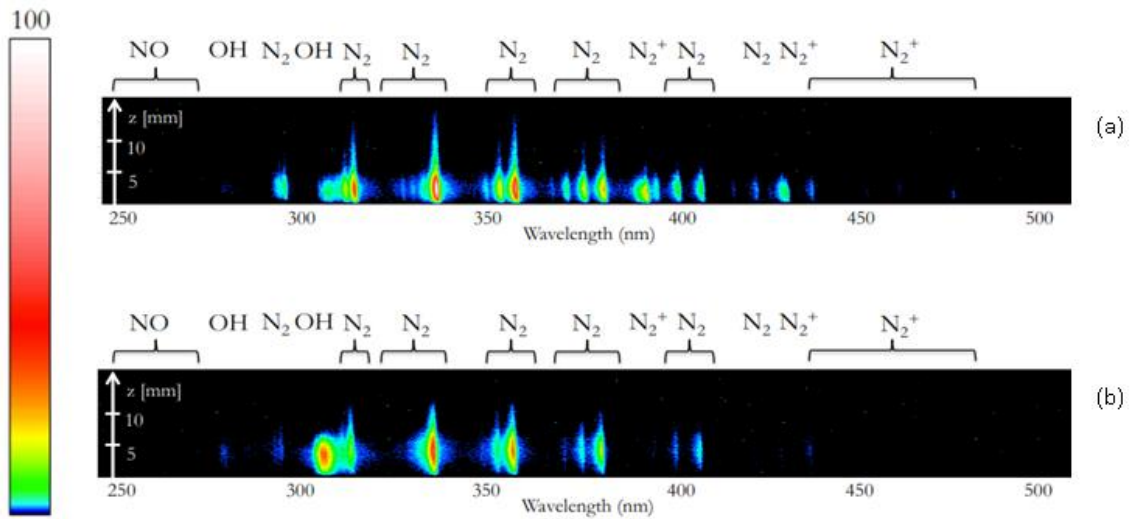


Fig. 2.14: Spatially resolved optical emission spectra of the plasma jet, operative conditions: primary gas He 1 slpm, PV 330 Hz, peak voltage 16 kV(a); primary gas Ar 1 slpm, PRF 330 Hz, peak voltage 16 kV (b)

Moreover, the role of the mass flow rate on the reactive species produced in the downstream region of the plasma jet is presented in Fig. 2.15 and Fig. 2.16; electrical operative conditions were set at 330 Hz and 20 kV for both cases. Comparing spectra for Ar as primary gas with mass flow rate at 1 slpm (Fig. 2.15a) and 5 slpm (Fig. 2.15b), the most notable result is the decrease of OH emission at higher mass flow rates; while, it should be noticed how the spatial region of OH emission is left unmodified by mass flow rate increase. On the other hand, increasing the primary gas mass flow rate from 1 slpm (Fig. 2.16a) to 5 slpm (Fig. 2.16b) in a He jet resulted in a stronger NO, OH and N_2^+ emission, while emission intensity for N_2 bands was unmodified. Unlike the Ar jet, the emitting region for the He jet extended further downstream as the mass flow rate was increased; finally, comparing Fig. 2.15 and Fig. 2.16, it should be noticed how NO and N_2^+ lines can be observed only for the He jet.

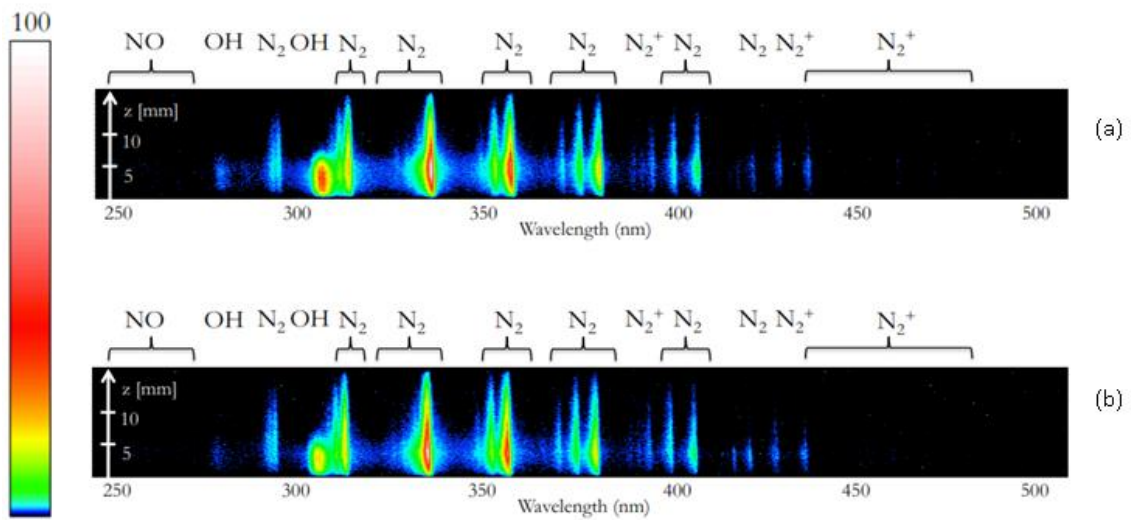


Fig. 2.15: Spatially resolved optical emission spectra of the plasma jet, operative conditions: primary gas Ar 1 slpm, PRF 330 Hz, PV 20 kV(a); primary gas Ar 5 slpm, pulse repetition frequency 330 Hz, peak voltage 20 kV(b)

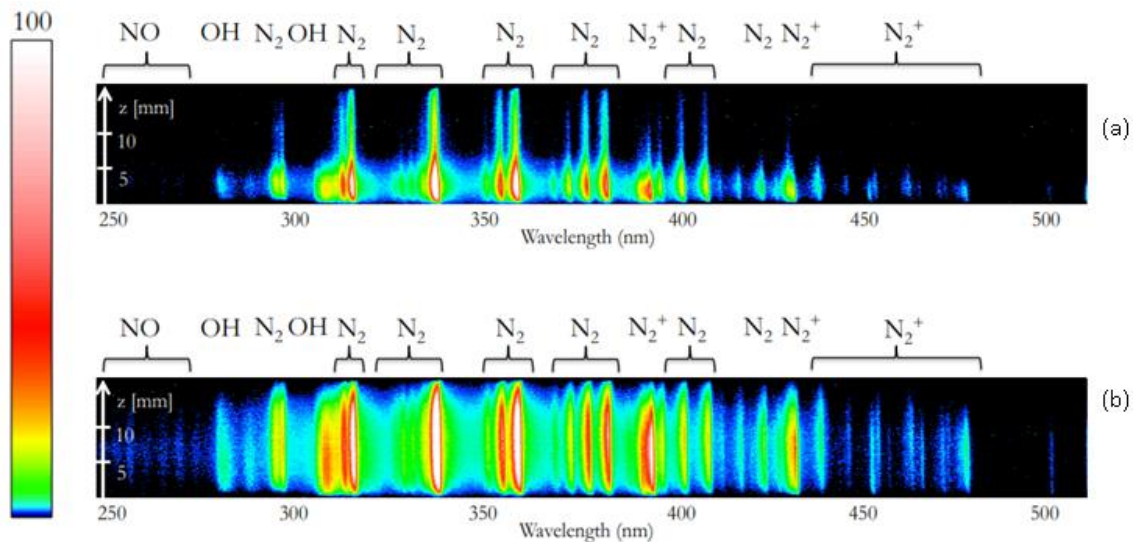


Fig. 2.16: Spatially resolved optical emission spectra of the plasma jet, operative conditions: primary gas He 1 slpm, PRF 330 Hz, PV 20 kV(a); primary gas He 5 slpm, PRF 330 Hz, peak voltage 20 kV(b)

The effects of peak voltage on the spectra emitted by the plasma jet are highlighted in Fig. 2.17, where two different configurations are compared using He as primary gas with a mass flow rate of 1 slpm and a pulse repetition frequency of 330 Hz.

Comparing spectra with peak voltage at 10 kV and 20 kV, the most notable results are higher emission intensity of OH, N₂, N₂⁺ and higher length of plasma emitting region, with the increase of peak voltage.

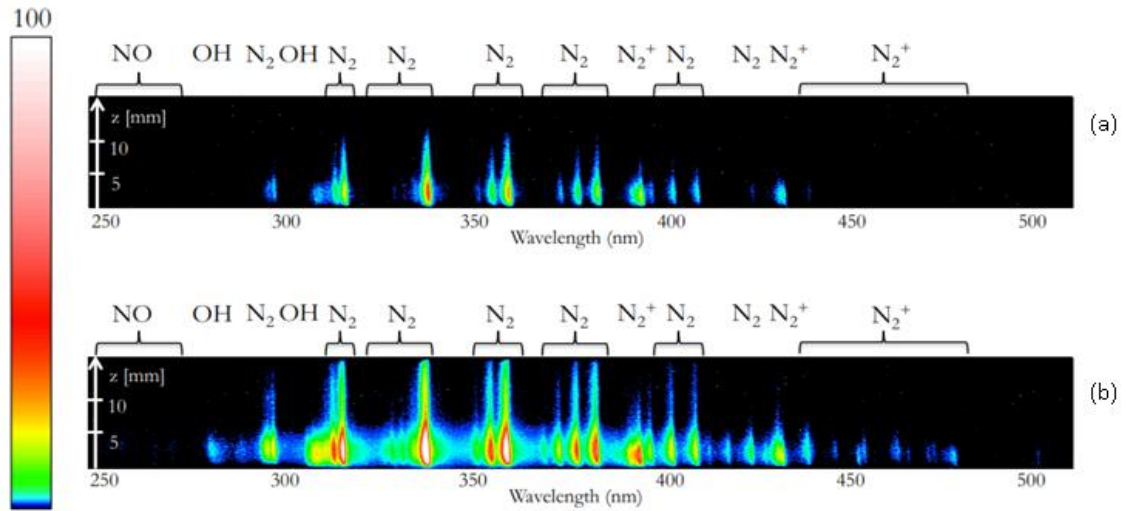


Fig. 2.17: Spatially resolved optical emission spectra of the plasma jet, operative conditions: primary gas He 1 slpm, PRF 330 Hz, PV 10 kV (a); primary gas He 1 slpm, PRF 330 Hz, PV 20 kV(b)

In Fig. 2.18, two configurations using He as primary gas, mass flow rate set at 1 slpm and peak voltage at 16 kV are adopted to show the role of frequency on reactive species production in the downstream region of the plasma jet. The increase of pulse repetition frequencies from 330 Hz to 1000 Hz resulted in an increase of OH and N₂⁺ emissions. Moreover, for every emitting species an increased pulse repetition frequency led to an extension of the region of peak emission.

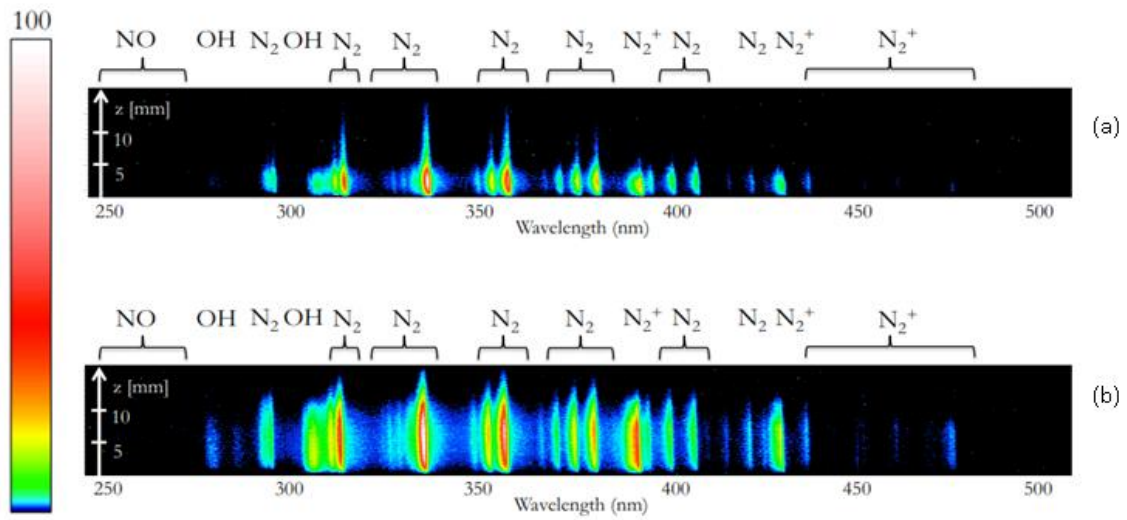


Fig. 2.18: Spatially resolved optical emission spectra of the plasma jet, operative conditions: primary gas He 1 slpm, PRF 330 Hz, PV 16 kV (a); primary gas He 1 slpm, PRF 1000 Hz, PV 16 kV (b)

Results for oxygen addition to the plasma jet are presented in Fig. 2.19, using He as primary gas with a mass flow rate of 5 slpm, a PRF of 1000 Hz and a PV of 16 kV. The addition of O₂ as secondary gas, with a mass flow rate 0.15 slpm, led to a decrease in the emission intensity of N₂ bands.

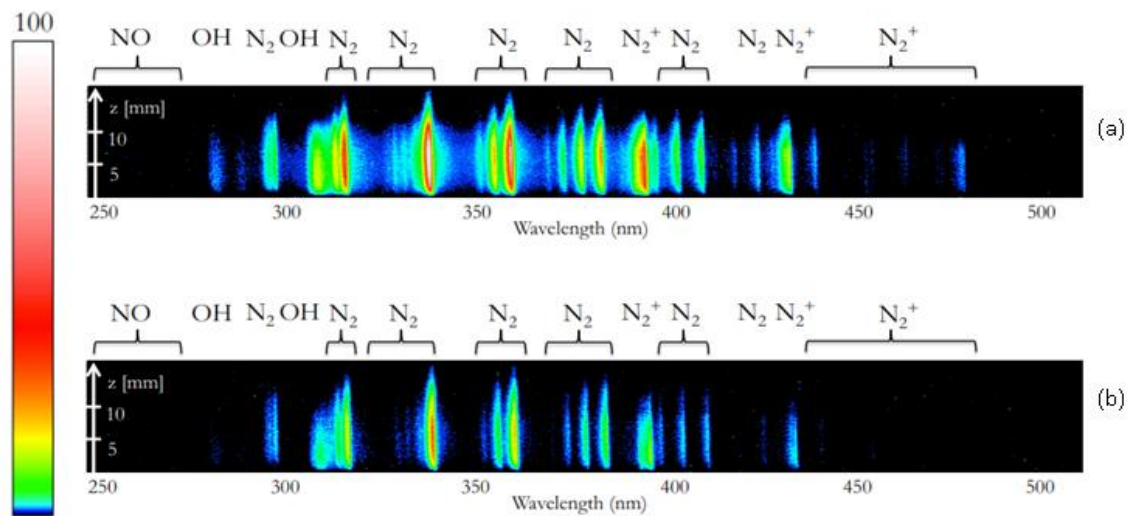


Fig. 2.19: Spatially resolved optical emission spectra of the plasma jet, operative conditions: primary gas He 5 slpm, PRF 1000 Hz, PV 16 kV (a); primary gas He 5 slpm, secondary gas O₂ 0.15 slpm, PRF 1000 Hz, PV 16 kV (b)

2.2.3.3 OES measurements in VIS-NIR range

Optical emission spectra in the VIS-NIR region from 500 up to 800 nm measured at different axial positions of the plasma jet at 330 Hz, 10 kV and a He primary gas flow rate of 5 slpm are shown in Fig. 2.20b, while a 0-dimensional spectrum for the same operative conditions at a fixed position is presented in Fig. 2.20a. Nitrogen bands were observed in the region between 675 and 760 nm as a consequence of second order diffraction, while lines of He were registered between 500 and 670 nm. A faint emission of O radicals was also observed at 777 nm.

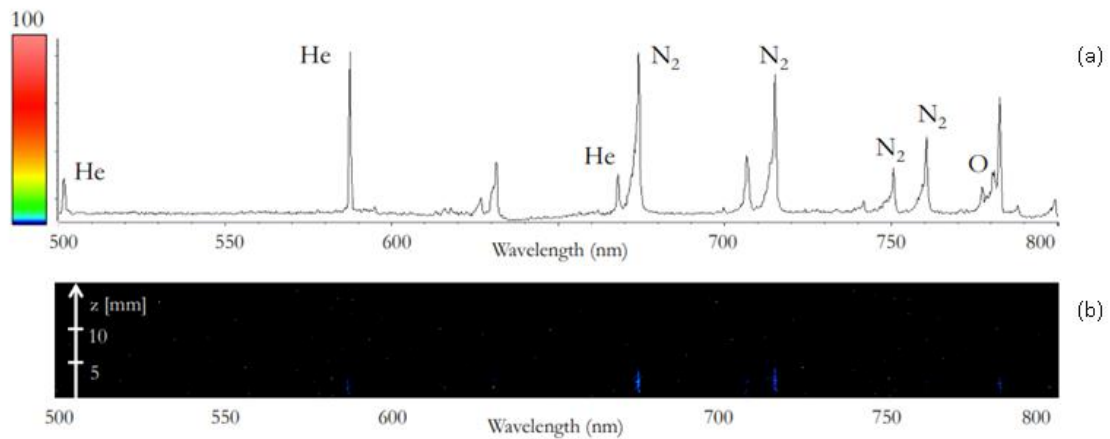


Fig. 2.20: Optical emission spectra of the plasma jet, operative conditions: primary gas He 5 slpm, PRF 330 Hz, PV 10 kV. Zero dimensional spectrum of the plasma jet at a distance 5 mm from the source outlet (a); spatially resolved spectra (b).

The effects of peak voltage on the spectra emitted by the plasma jet are highlighted in Fig. 2.21, where two different configurations are compared using He as primary gas, with a mass flow rate of 1 slpm and a pulse repetition frequency of 330 Hz.

Comparing spectra with peak voltage at 20 kV and 10 kV, a strong increase of emission intensity of He, N₂, O lines is observed for the case at 20 kV. Moreover, for the 20 kV peak voltage case He and O lines are very intense at the jet outlet, while for N₂ lines maximum intensity was measured few millimeters downstream the source outlet.

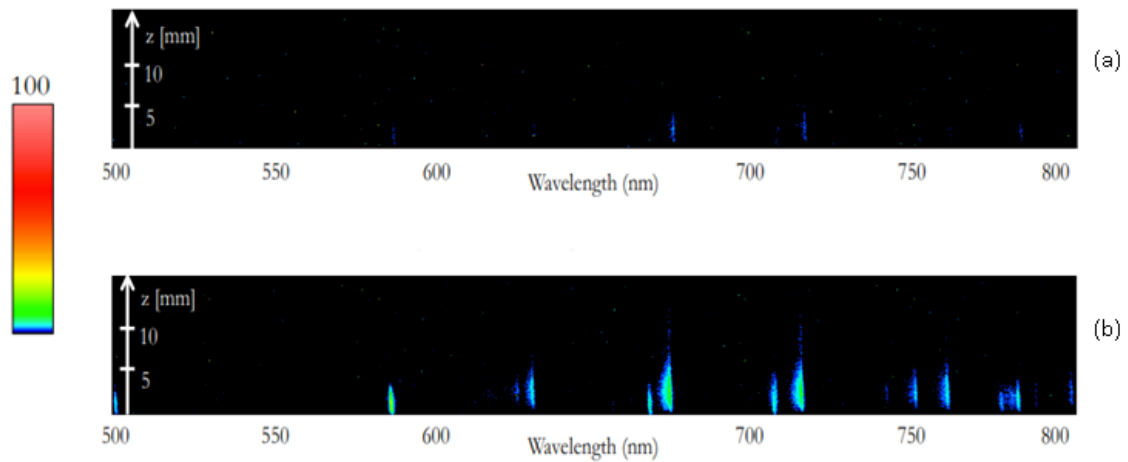


Fig. 2.21: Spatially resolved optical emission spectra of the plasma jet, operative conditions: primary gas He 1 slpm, pulse repetition frequency 330 Hz, PV 10 kV (a); primary gas He 1 slpm, PRF 330 Hz, peak voltage 20 kV (b)

Moreover, the role of mass flow rate on the variety of reactive species produced in the plasma jet is presented in Fig. 2.22, where two different configurations are compared, using He as primary gas with a mass flow rate of 5 slpm, a PRF of 1000 Hz and a PV of 16 kV, adding in one of these configurations O_2 as secondary gas with a mass flow rate 0.15 slpm. The most notable result is a lower emission intensity of N_2 bands and a slightly higher O emission, in the case of O_2 addition.

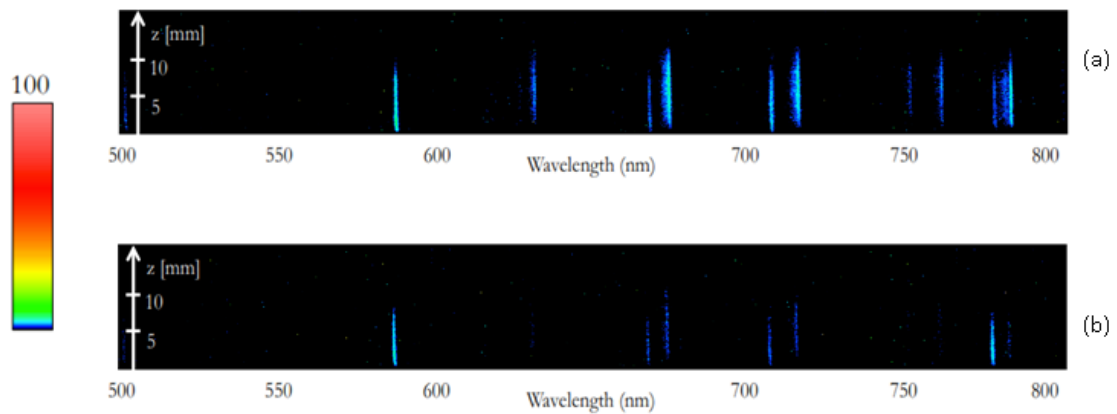


Fig. 2.22: Spatially resolved optical emission spectra of the plasma jet, operative conditions: primary gas He 5 slpm, PRF 1000 Hz, PV 16 kV (a); primary gas He 5 slpm, secondary gas O₂ 0.15 slpm, PRF 1000 Hz, PV 16 kV (b)

An increase of peak voltage and pulse repetition frequency was found to produce an increase in the length of the emitting region of the plasma plume and the concentration of reactive species. The effect of peak voltage increase can be explained in terms of the higher local electric field produced in the plasma plume which, in turn, produces a higher electron concentration that enhance the production of excited species and radiation emission[1].

A higher emission of OH lines has been measured for Ar primary gas, while the addition of O₂ secondary gas was found to decrease the overall emissivity of the plasma.

2.2.4 Temperature and heat flux measurements

Temperature measurement in the downstream region of the nanosecond pulsed jet were carried out by means of fiber optic temperature sensors. The same sensors was also be used to measure the heat flux of the jet as proposed in [19]. Axial and

radial trends of plasma jet temperature and heat fluxes, for different values of primary gas mass flow rates, peak voltage and pulse repetition frequency and for different plasma gas compositions are reported.

2.2.4.1 Temperature and heat flux measurements setup

Axial and radial temperature distribution and heat flux profiles of the plasma jet were measured by means of a fiber optic temperature sensor (OPSENS OTP – M) with a calibration range of 20 °C – 60 °C, a 0.001 °C resolution, an 0.15 °C accuracy and a response time of less than 1 s; a second fiber optic sensor was employed to monitor room temperature during the measurements, as schematically presented in Fig. 2.23.

Axial heat flux was measured exposing a copper substrate, with a surface of 0.65 cm² and a weight of 0.15 g, to the jet plasma source at different distances from its tip and monitoring its temperature with a fiber optic temperature sensor. Therefore the heat flux to the copper substrate was calculated from its measured temperature increase in a time lapse of 0.9 s as done in [19] by means of this simple balance equation

$$Q = \frac{m \cdot c_w \cdot \frac{\Delta T}{\Delta t}}{A}$$

where Q is the heat flux, m the copper substrate weight, c_w the copper specific heat, ΔT the temperature increase of the copper substrate, Δt the duration of plasma exposure and A the surface of the copper substrate.

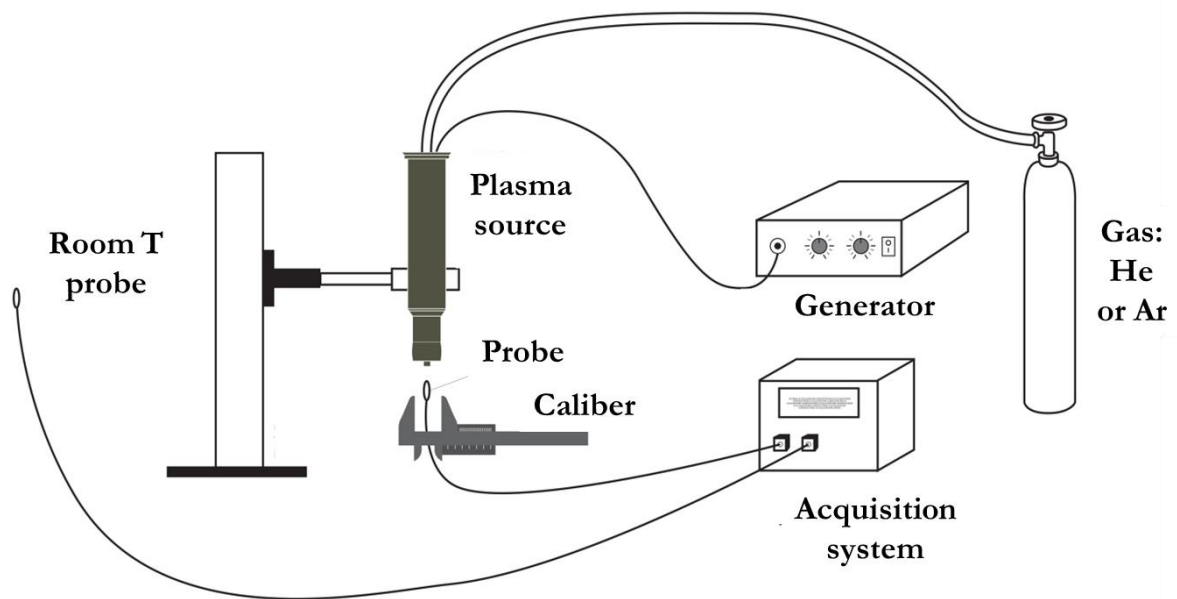


Fig. 2.23: Schematic of the diagnostic apparatus for the determination of temperature and heat flux profiles

2.2.4.2 Axial and radial temperature profiles of the plasma jet

Fiber optic sensors was used to measure the axial and radial temperature profiles of the plasma jet for different primary gas compositions, primary gas mass flow rates, peak voltages and pulse repetition frequencies. As shown in Fig. 2.24, using He instead of Ar as primary gas results in a considerably higher axial temperature (operating conditions: primary gas 1 slpm, pulse repetition frequency 1000 Hz, peak voltage 17 kV). In the case with Ar the measured temperatures have shown negligible differences from room temperature.

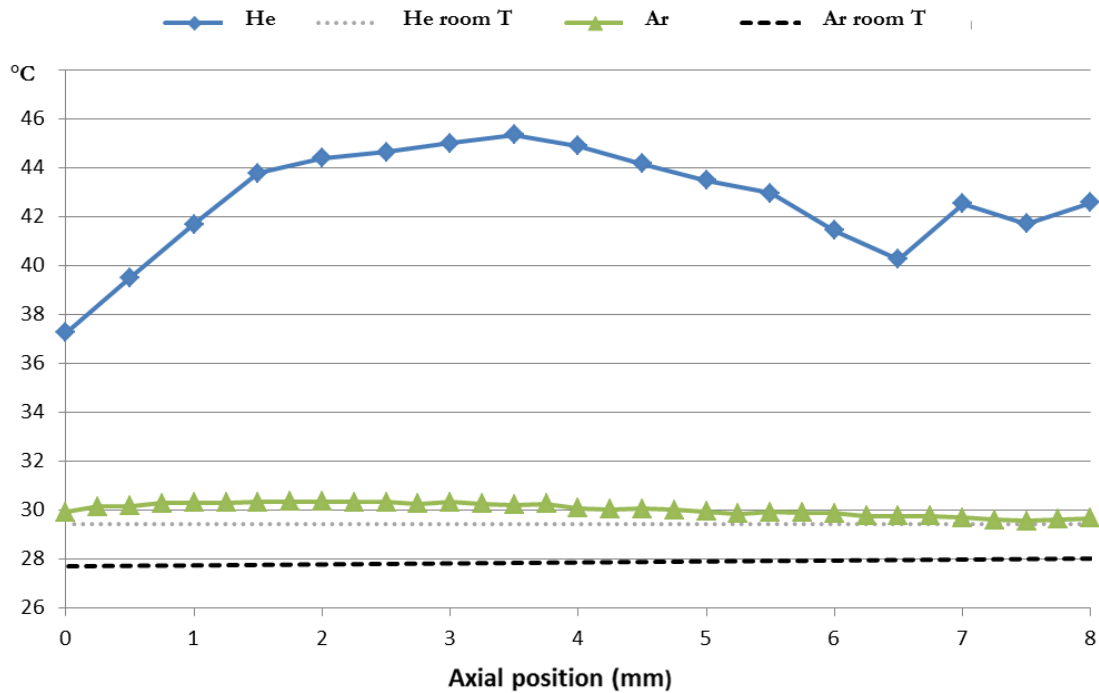


Fig. 2.24: Axial temperature profiles of the plasma jet, operating conditions: primary gas He 1 slpm (blue) or gas Ar 1 slpm (green), PRF 1000 Hz, PV 17 kV (blue). Room temperature during measurements in the He case (dotted line) and Ar case (dashed line), respectively.

The effect of the He flow rate on the axial temperature of the plasma jet is highlighted in Fig. 2.15. Measurements of the temperature profile were carried out for the jet driven by nanosecond pulsed high voltage power supply; and two different He flow rate: 1 slpm to 3 slpm. For the 1 slpm case, a drastic decrease of the axial temperature was observed 10 mm downstream plasma source outlet, while in the 3 slpm case the axial temperature profile presented only small deviations around the mean value from the jet, close to the room temperature. Interestingly, also the visible plasma plume outside the plasma jet is shorter for the case at 1 slpm, as shown in Fig. 17.

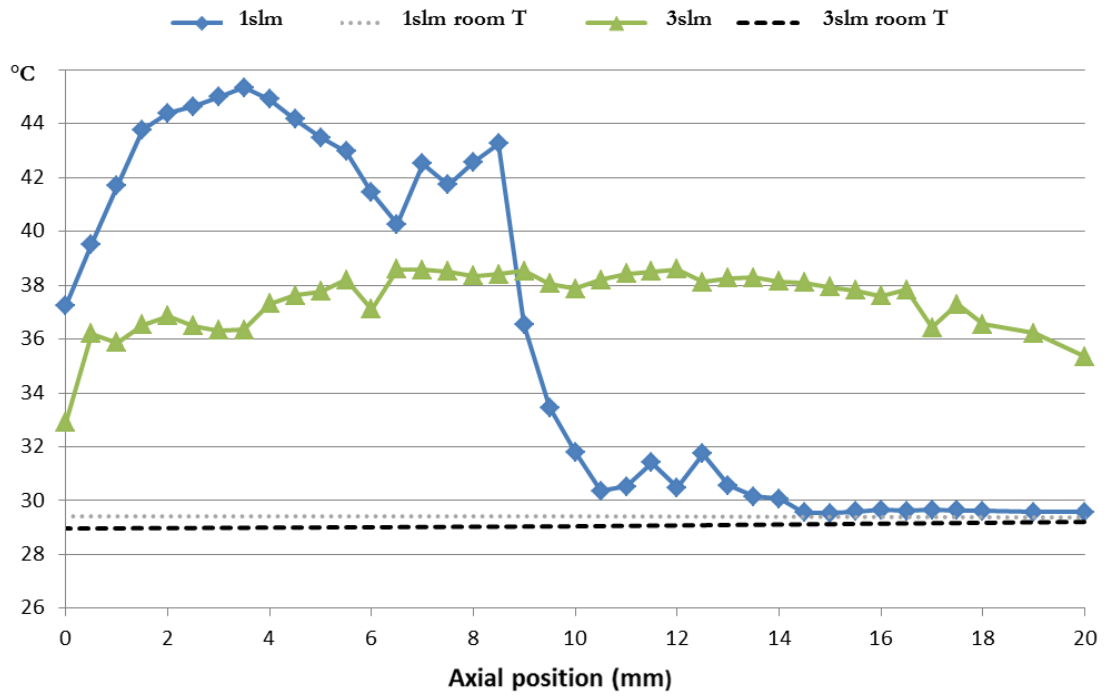


Fig. 2.25: Axial temperature profiles of the plasma jet, operating conditions: primary gas He 1 slpm, pulse repetition frequency 1000 Hz, peak voltage 17 kV (blue); primary gas He 3 slpm, pulse repetition frequency 1000 Hz, peak voltage 17 kV (green). Room temperature during measurements of the 1 slpm case (dotted) and of the 3 slpm case (dashed), respectively.

The effects of peak voltage on plasma jet axial temperature distribution are highlighted in Fig. 2.26; increasing the peak voltage from 14 kV to 17 kV, while keeping constant primary gas mass flow rate (Ar, 3 slpm) and pulse repetition frequency (1000 Hz), resulted in an almost constant rise of temperature along the plasma plume. Similar results were been observed increasing pulse repetition frequency from 500 Hz to 1000 Hz maintaining constant primary gas mass flow rate (Ar, 3 slpm) and peak voltage (14 kV), as shown in Fig. 2.27.

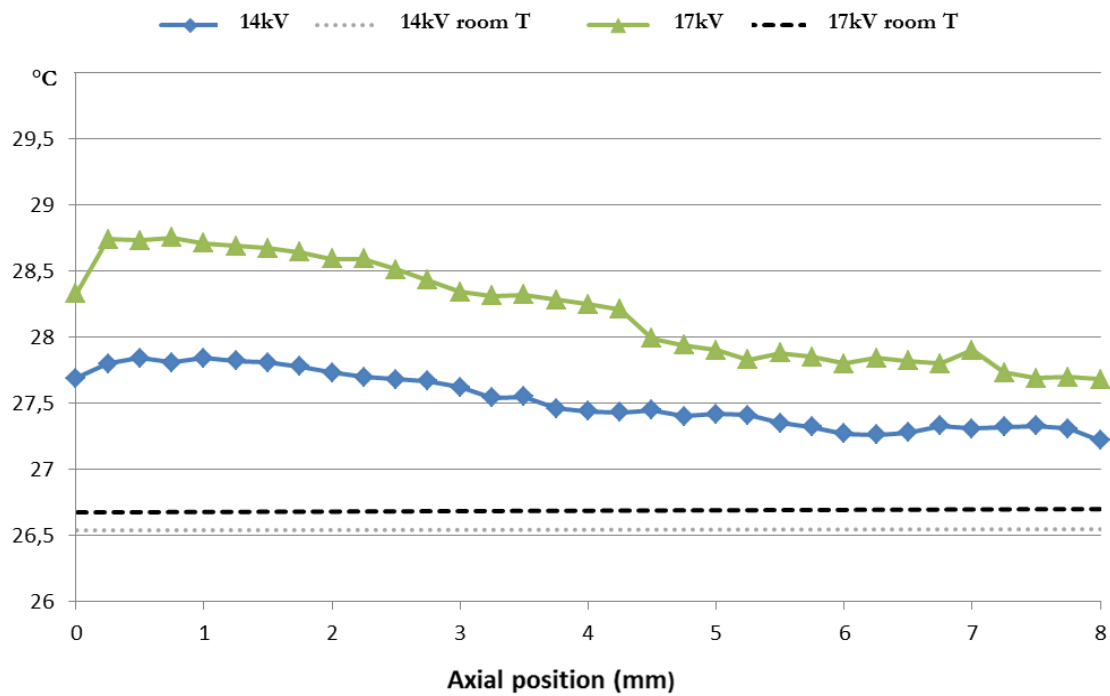


Fig. 2.26: Axial temperature profiles of the plasma jet, operating conditions: primary gas Ar 3 slpm, PRF 1000 Hz, peak voltage 14 kV (blu) or PV 17 kV (green). Room temperature during measurements of the 14 kV case (dotted) and of the 17 kV case (dashed)

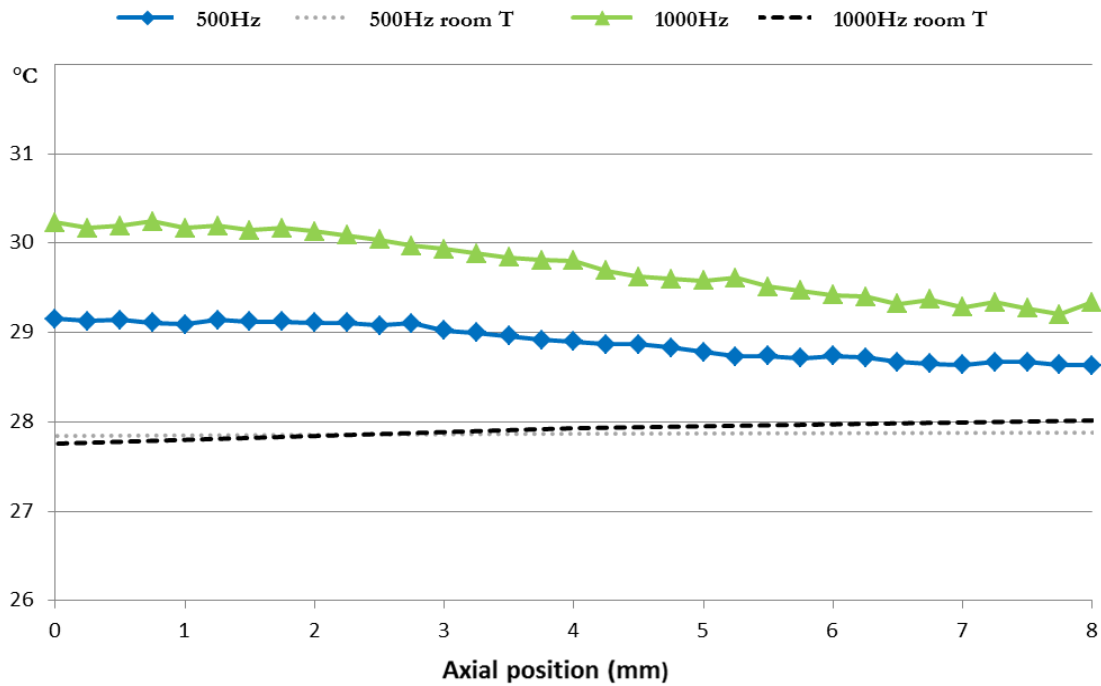


Fig. 2.27: Axial temperature profiles of the plasma jet, operating conditions: primary gas Ar 3 slpm, PRF 500 Hz, PV 14 kV (blue); primary gas Ar 3 slpm, PRF 1000 Hz, PV 17 kV (green). Room temperature during measurements of the 500 Hz case (dotted) and of the 1000 Hz case (dashed)

Measurements of radial temperature distribution in the jet were collected at different distances from the outlet, as shown in Fig.2.28. The effect of the primary gas composition on the radial temperature distribution in the jet is shown in Fig. 2.29, where results for 5 slpm of He (Fig. 2.29a) and 3 slpm of Ar (Fig. 2.29b) are compared; pulse repetition frequency is set at 500 Hz and peak voltage at 14 kV in both configurations. With 5 slpm of He as primary gas, the maximum temperature was found to be almost on the axis of the plasma jet, 1 mm downstream the outlet; on the other hand, the jet radial temperature profile for the Ar case shows almost no variation from room temperature.

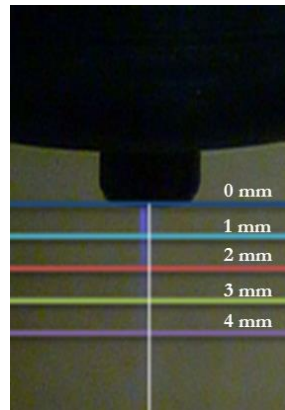


Fig. 2.28: Schematic for the different axial distances from the nozzle where radial temperature profiles of the plasma jet are measured

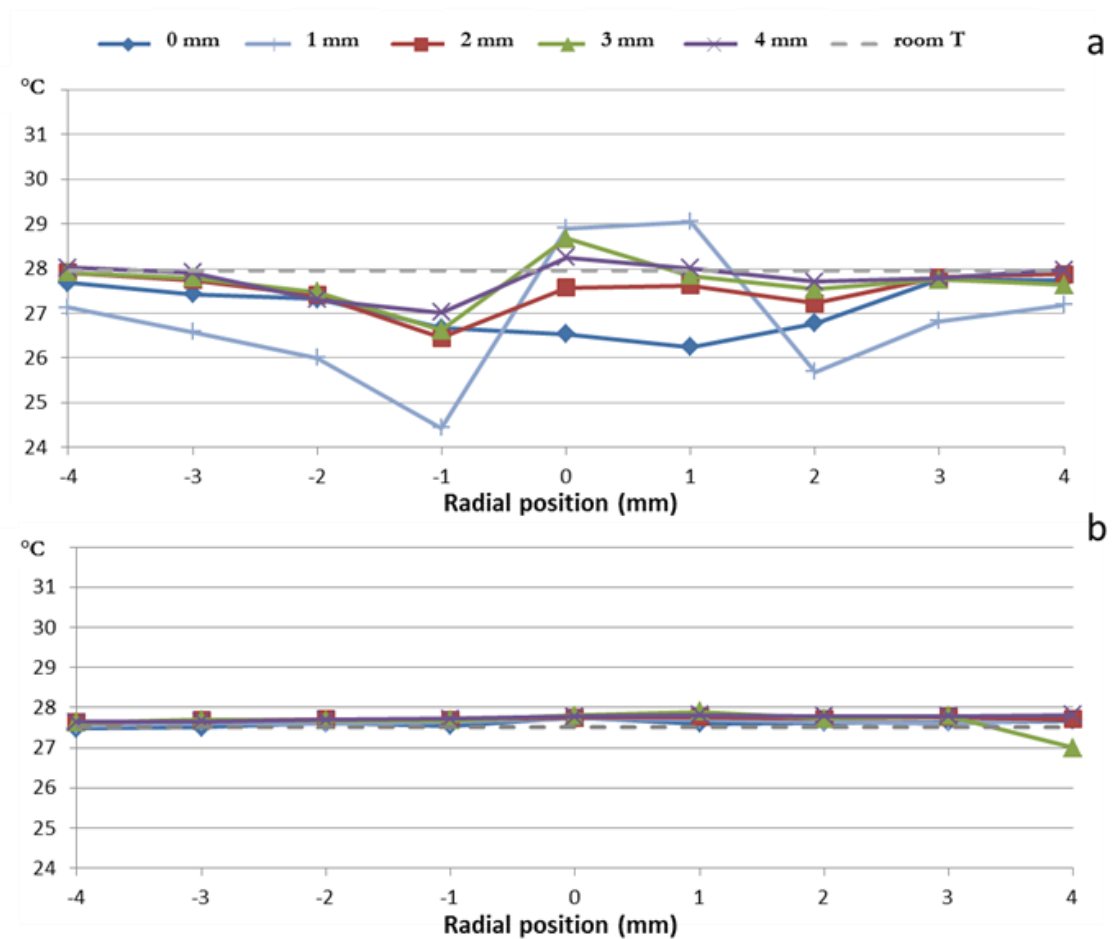


Fig. 2.29: Radial temperature profiles of the plasma jet evaluated for different operating conditions: primary gas He 5 slpm, PRF 500 Hz, PV 14 kV (a); primary gas Ar 3 slpm, PRF 500 Hz, PV 14 kV (b). Room temperature (dashed line)

As previously shown for axial temperature measurements, increasing the peak voltage from 14 kV to 17 kV resulted in a rise of radial temperature, especially near the axis of the jet; results for He as primary gas with a mass flow rate of 5 slpm and a pulse repetition frequency of 1000 Hz are shown in Fig. 2.30.

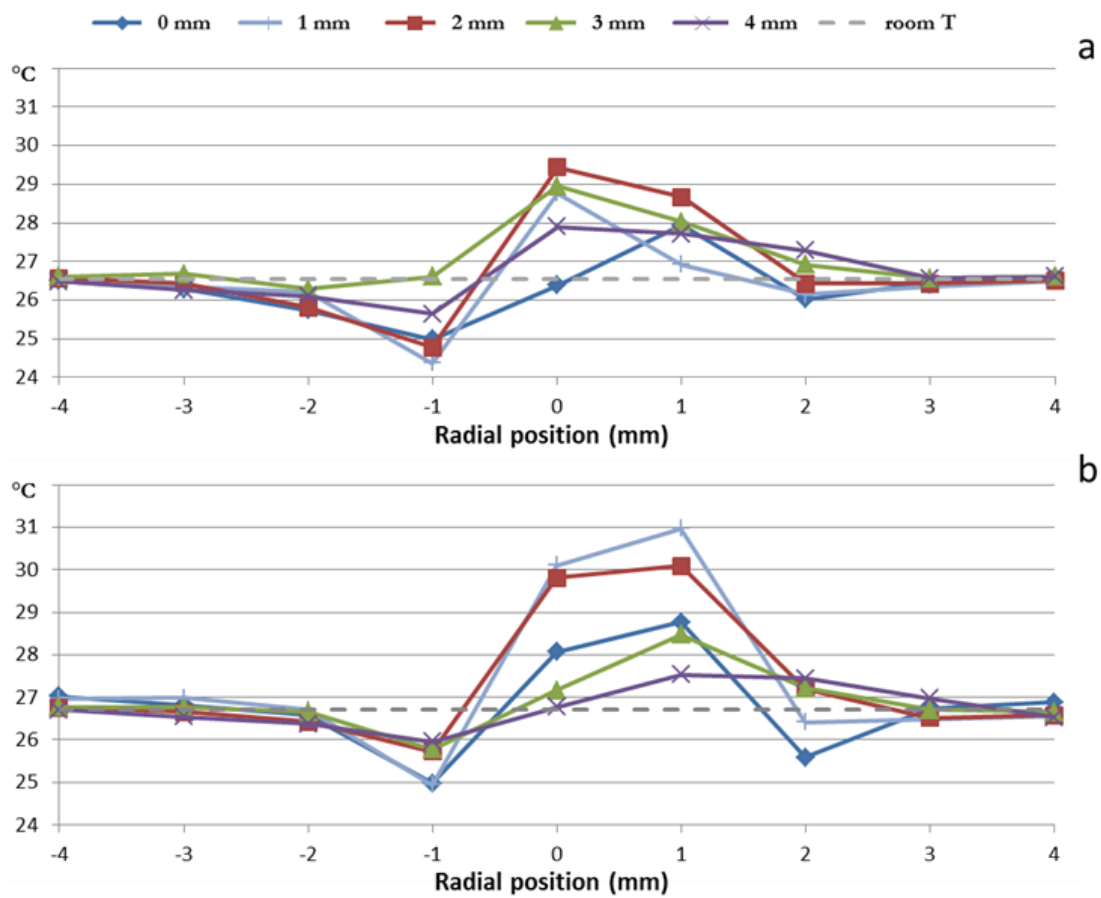


Fig. 2.30: Radial temperature profiles of the plasma jet evaluated at different axial distances from the nozzle (c), operating conditions: primary gas He 5 slpm, PRF 1000 Hz, PV 14 kV (a); primary gas He 5 slpm, PRF 1000 Hz, PV 17 kV (b). Room temperature (dashed line)

Finally, the effect of frequency is pointed out in Fig. 2.31, where measurements of the plasma jet operated in two configurations using He as primary gas, mass flow rate set at 5 slpm and peak voltage at 14 kV are presented; similarly to increasing peak voltage, a rise of pulse repetition frequencies from 500 Hz to 1000 Hz resulted in a slight increase of peak temperature in the region in the proximity of the axis of the jet.

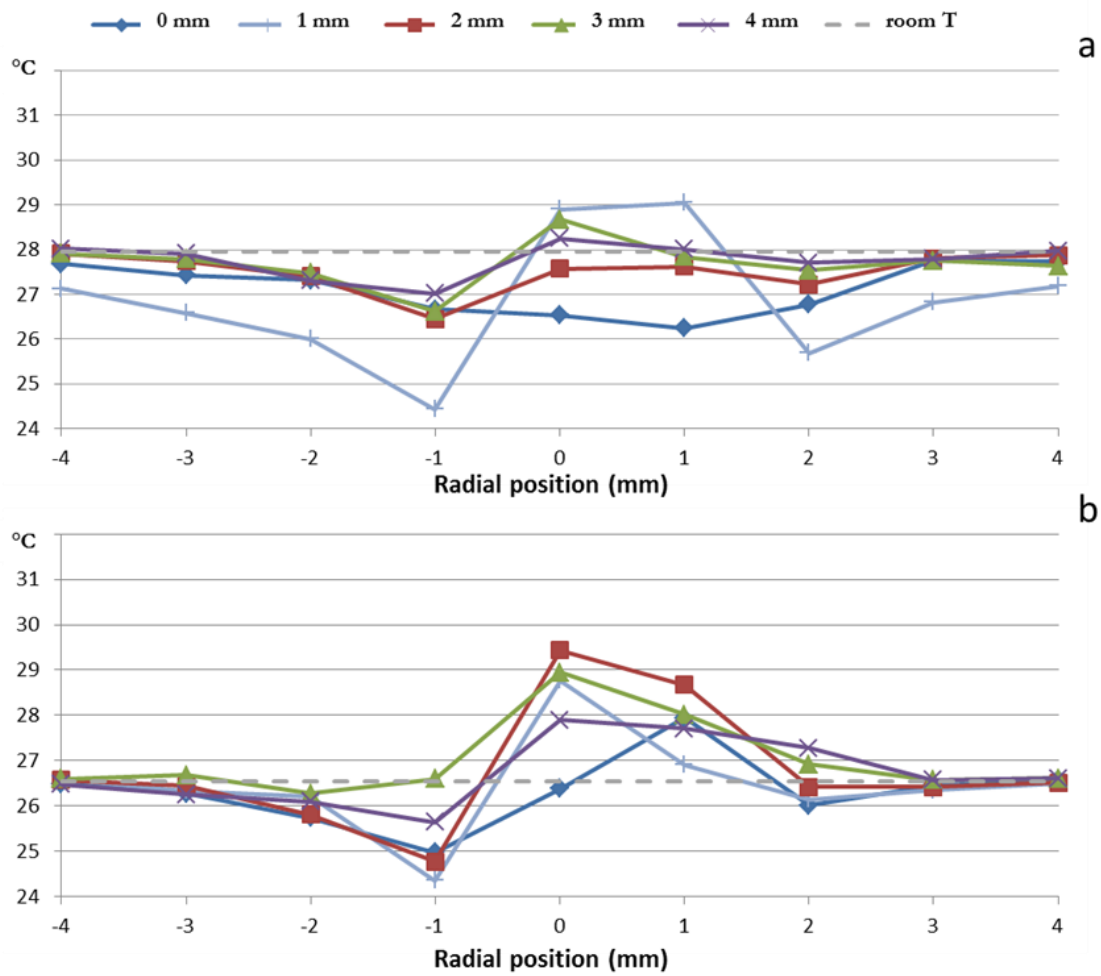


Fig. 2.31 Radial temperature profiles of the plasma jet evaluated at different axial distances from the nozzle (c), operating conditions: primary gas He 5 slpm, PRF 500 Hz, PV 14 kV (a); primary gas He 5 slpm, PRF 1000 Hz, PV 14 kV (b). Room temperature (dashed line)

2.2.4.3 Heat flux measurement

As expected from temperature profiles, a very limited axial heat flux from the plasma jet with Ar as primary gas was found; indeed, an axial heat flux below 0.02 W/cm^2 along the whole axis of the plasma plume is shown in Fig. 2.32 for the following operating conditions: mass flow rate 3 slpm, pulse repetition frequency 500 Hz and peak voltage 14 kV.

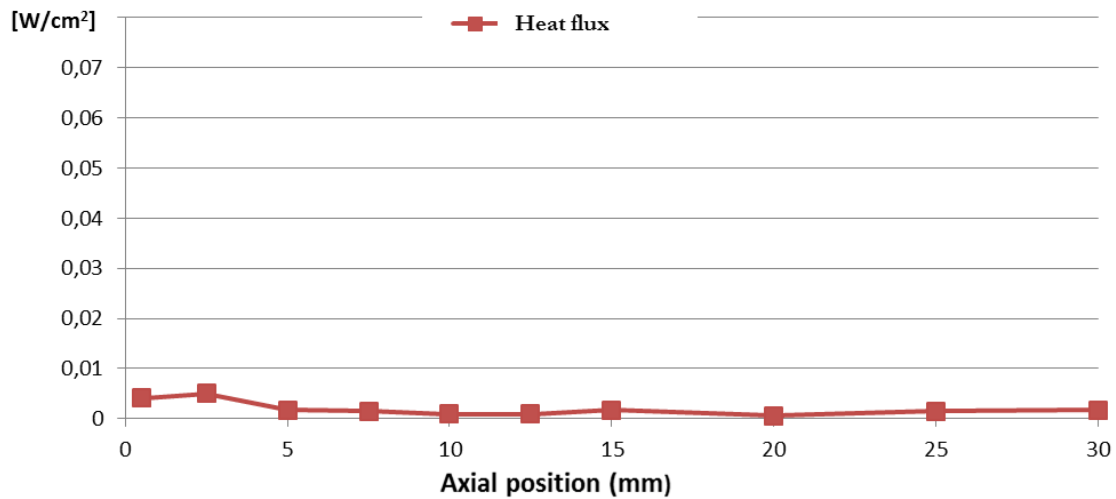


Fig. 2.32: Axial heat flux profile of the plasma jet, operating conditions: primary gas Ar 3 slpm, PRF 500 Hz, PV 14 kV

He has been employed as the primary gas to investigate the effect of the mass flow rate on axial heat flux, whose profiles are shown in Fig. 2.33 for a pulse repetition frequency of 500 Hz and a peak voltage of 14 kV; interestingly, even if the increase of the mass flow rate causes a decrease of the axial temperature peak, it also induces an increase of the axial heat flux as a combination of the higher mean temperature of the jet and the higher mass flow rate itself. The maximum heat flux of 40 mW/cm^2 was

measured for the case with 5 slpm of He, a significantly low value when compared to other plasma sources for biomedical applications [19].

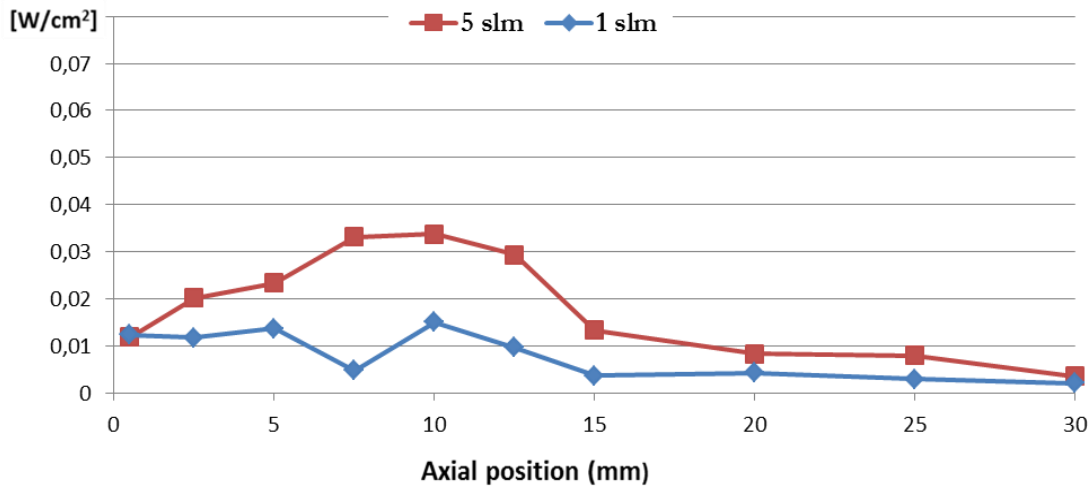


Fig. 2.23: Axial heat flux profiles of the plasma jet, operating conditions: primary gas He 5 slpm, PRF 500 Hz, PV 14 kV (red); primary gas He 1 slpm, PRF 500 Hz, PV 14 kV (blue)

While both the radial and axial temperature profiles of the Ar plasma jet were found to hardly differ from the room temperature, higher temperatures have been measured for the He plasma jet; for the latter case, an increase of pulse repetition frequency and voltage peak resulted in a rise of the temperature of the plasma jet. Finally, a very limited maximum axial power density (below 40 mW/cm²) transferred from the plasma jet has been measured for the case of He as the primary gas, while in the Ar case the calculated heat flux is lower than 0.02 mW/cm².

2.3 Plasma enhanced electrospinning

Electrospinning is a versatile technology that allows the fabrication of non-woven mats made in polymeric or inorganic fibers having dimensions ranging from tens of micrometers to a few. The electrospinning process is based on jets of an electrostatically charged molten polymer or of a polymeric solution collected on grounded plates or rolls [41]. The electrospinnability of the polymeric solution strongly depends on rheological properties, electrical conductivity and surface tension [42, 43]. Specifically, high viscosity, high charge density and low surface tension interplay in the formation and evolution of the electrospinning jet and are key factors in controlling fiber morphology and in producing bead-free fibers [44]. The presence of undesired defect along the fiber axis (beads) worsens mat mechanical properties, being commonly responsible of mat increased fragility [45]. Most polymers have low dipole moments and can be dissolved only in non-polar solvents that are not suitable, however, for electrospinning purposes due to their low dielectric constant. In these cases, the improvement of the electrospinnability of the solution can be reached with the addition of a proper amount of highly polar solvents or salts to increase dielectric constant and conductivity of polymeric solution [46, 47]. However, this addition causes additional costs, safety and environmental concerns. Moreover, complete evaporation of highly polar solvents, having low vapour tension, cannot be assured during the electrospinning process, so traces of the solvent could be found in the produced mats [48]: this causes big problems in the use of the electrospun mats in the biological field,

where toxic solvent evaporation during the path from the tip of the needle to the grounded electrode must be maximized.

Recently, Shi et al. demonstrated that atmospheric plasma treatment can increase the electrospinnability of an aqueous polymeric solution [49]. In particular, if poly(ethylene oxide) (PEO) water solution is exposed to a DBD plasma before the electrospinning process, the fiber morphology in the final mat is significantly improved, leading to nanofibers possessing a lower amount of beads with respect to fibers produced from an untreated solution. The plasma treatment can induce the ionization of polymer chains and solvent molecules, causing an increase of conductivity, viscosity and surface tension of the polymeric solution [49]; the increase of charges in the treated solution induces the conductivity, while the intramolecular interaction is affected by the presence of solvent and polymer ionized molecules, increasing the viscosity and surface tension of the solution. While plasma phenomena occurring in aqueous solutions are being thoroughly investigated [50, 51], only few works focus on the interaction between plasma and liquids different from water; as examples, reduction of silver nitrate in a solution of polyacrylonitrile (PAN) dissolved in N,N-dimethylformamide (DMF) to produce Ag nanoparticles was induced by means of a plasma treatment [52], while plasma discharges generated in mineral oil was demonstrated to completely crack organic molecules [53].

In this chapter, the effect of the exposure of a poly(L-lactic acid) (PLLA) solution in dichloromethane (DCM) to the argon plasma jet [54] on the solution electrospinnability is investigated. PLLA is a biocompatible and biodegradable polymer and can be solved in non-polar organic solvents, such as DCM with the addition of an

appropriate amount of polar non solvents, such as DMF, to increase the dielectric constant of the solution [55,56]. However, the boiling temperature of DMF is around 153°C, while the DCM one is about 40°C, and therefore it might be difficult to assure the complete evaporation of the DMF during the electrospinning process in order to completely avoid traces of residual DMF in the scaffold after the electrospinning process, as previously mentioned.

2.3.1 Electrospinning process

The electrospinning apparatus, made in house and schematically represented in fig. 2.24, was composed of a high voltage power supply (Spellman, SL 50 P 10/CE/230), a syringe pump (KDScientific 200 series), a glass syringe, a stainless steel blunt-ended needle (inner diameter: 0.84mm) connected with the power supply electrode and a grounded aluminium plate-type collector (7×7 cm²). The polymer solution was dispensed through a Teflon tube to the needle, vertically placed on the collecting plate. PLLA solutions were electrospun by using the following conditions: voltage = 15 kV, needle-to-collector distance = 15 cm, flow rate = 0.015 ml/min [36].

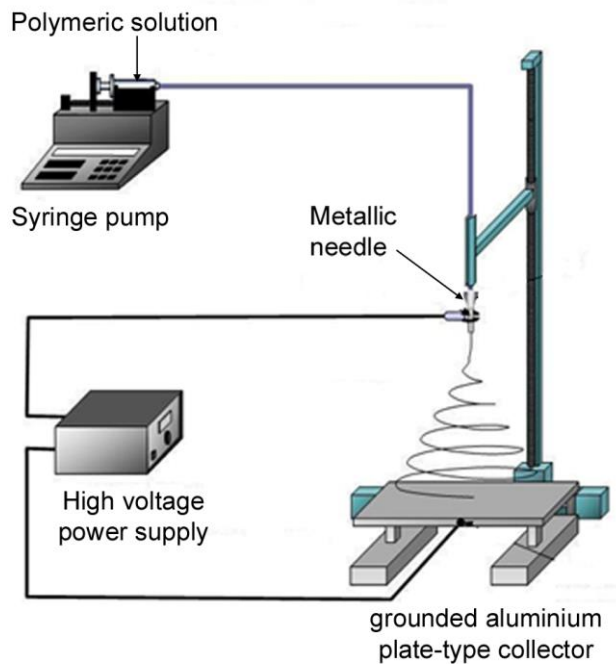


Fig.2.24 Schematic of the electrospinning apparatus [36]

Poly(L-lactic acid) (PLLA) (Lacea H.100-E) ($M_w = 8.4 - 104 \text{ g/mol}$, $PDI = 1.7$) was supplied by Mitsui Fine Chemicals. Dichloromethane (DCM) was purchased by Sigma–Aldrich and it was used without any further purification.

Scanning Electron Microscope (SEM) observations were carried out using a Philips 515 SEM by applying an accelerating voltage of 15 kV on samples sputter coated with gold. The distribution of fiber diameters was determined through the measurement of about 200 fibres by means of an acquisition and image analysis software (EDAX Genesis), and the results were given as the average diameter \pm standard deviation.

2.3.2. Plasma treatment of polymeric solution

The plasma source was driven by two different power supplies: a pulse generator (FID GmbH – FPG 20-1NMK) producing high voltage pulses with a slew rate of few kV/ns, a peak voltage of 7-20 kV into a 100-200 Ω load impedance and a maximum pulse repetition rate of 1000 Hz and a HVAmplifier (Trek model 30/20-H-CE, ± 30 kV, 20mA) connected to a function generator (Stanford Research model DS335, 3 MHz), as previously described. The polymeric solution was spilled in a weighing bottle glass and exposed to the plasma source for different treatment times and operating conditions. A stand off of 5 mm and an Ar flow rate of 2 slpm was fixed for all the treatments.

The plasma treatment was performed for different treatment times and operating conditions on a polymeric solution spilled in a pre-weighted glass vial without cap. Depending on the working conditions (PV, PRF, distance between the electrode and the liquid surface, working gas) the single electrode plasma jet can be operated either in glow or streamer regime [50] as shown in Fig. 2.25 in the case of a water interface. Since a negligible improvement of solution electrospinnability was found when operating in the glow-discharge regime, only results regarding the streamer regime treatments will be presented. The treatment was performed by randomly moving the source at constant stand-off, maintaining a streamer behaviour of the discharge during the process [57].

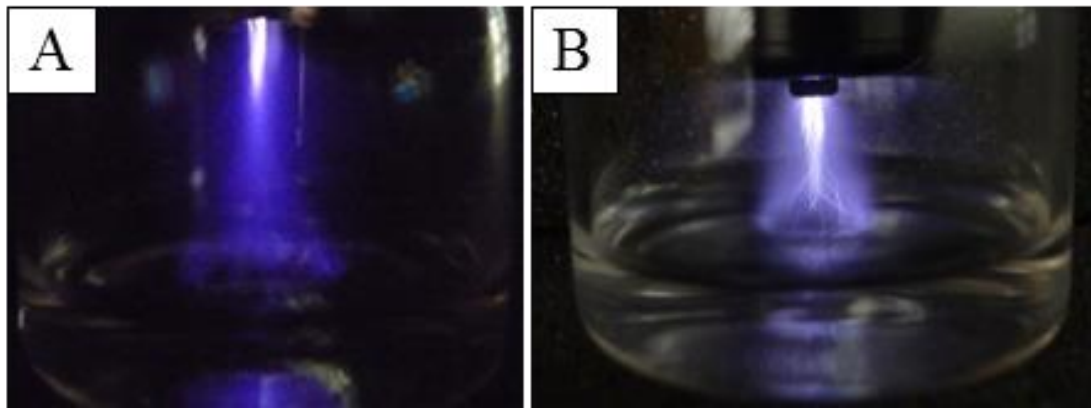


Fig. 2.25 Plasma treatment on water: glow regime (A), streamer regime (B) [36]

The weight of the polymeric solution before and after plasma treatment was measured by means of an electronic balance (Radwag PS600/C/2), in order to evaluate possible change of polymeric solution concentration due to solvent evaporation.

In order to evaluate the effects of plasma treatment on the electrospinnability of PLLA, SEM images were analysed focusing on mat fiber morphology (fiber diameter distribution and presence of beaded defects along the fiber axis).

In particular, comparison between the morphologies of control non-woven mats electrospun from untreated PLLA solutions and of mats fabricated from PLLA solutions exposed to plasma was performed.

In fig.2.26, SEM images of PLLA mats obtained from solutions at different polymer concentration (8% w/v, 10% w/v, and 13% w/v) in 100% DCM and a solution at 13 w/v in DCM:DMF=65:35 are presented. If the electrospinning solution consists of PLLA in plain DCM, the formation of non-uniform fibers with a large number of defects that weakened the mat preventing its peeling off from the collecting plate occurs,

while the addition of 35% vol of DMF to DCM allows the production of mat made of fibers without defects and mechanically resistant [55].

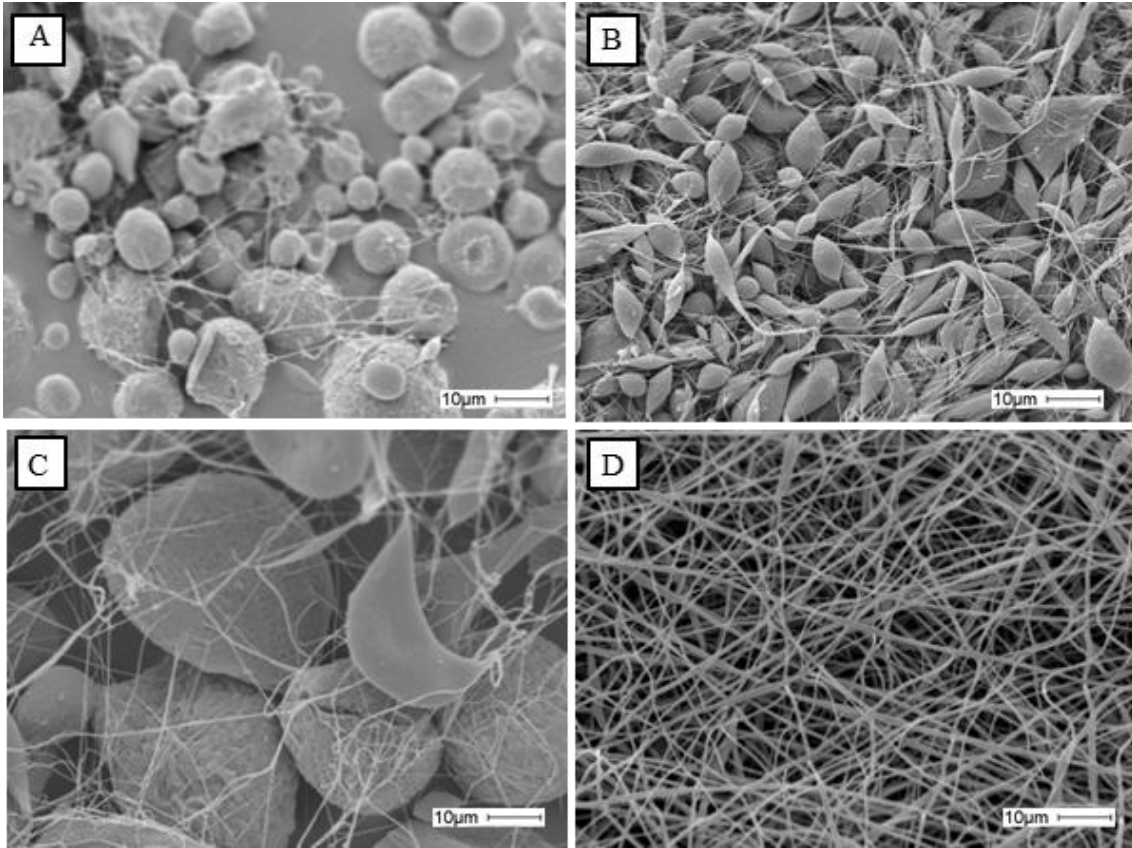


Fig. 2.26 SEM images of control mats obtained without plasma treatment of the electrospinning solution: PLLA dissolved at a concentration of 8% w/v (A), 10% w/v (B) and 13% w/v (C) in 100% DCM; PLLA dissolved in DCM:DMF=65:35 (v/v) at a concentration of 13% w/v (D). Magnification: 1000 X [36]

The effect of different plasma treatments on electrospinnability of 10% w/v PLLA solution dissolved in pure DCM was evaluated: the plasma jet was generated and sustained using different voltage waveforms, as reported in Table 1.

PRF [kHz]	V _{pp} [kV]	Waveform shape	Polarity	Treatment time [s]
1	+20	Square	Homopolar	120
1	-20	Square	Homopolar	120
1	+20	Square	Homopolar	10
1	+20	Square	Non Homopolar	120
1	+40	Square	Non Homopolar	120
1	+20	Sinusoidal	Homopolar	120
1	+20	Sinusoidal	Non Homopolar	120
1	+20	Triangular	Homopolar	120
1	+20	Triangular	Non Homopolar	120
1	+20	Sawtooth	Homopolar	120
1	+20	Nanopulsed	Homopolar	10
1	+20	Nanopulsed	Homopolar	120

Table 1. Electrical operating conditions and exposure times [57]

The electrospinnability improvement induced by the plasma treatment strongly depends on the high voltage waveform driving the plasma jet. Different mats have been collected at different times since the beginning of the electrospinning processes, in order to highlight the decrease of the treatment effect in the time.

An exposure time of 120 seconds to the plasma jet driven by nanosecond pulsed voltage waveform allowed the production of a mat made of defect free nanofibers (Fig.2.27 A). If the polymeric solution is electrospun 210 minutes after the plasma treatment, beads formation occurs as shown in Fig. 2.27 A'. In order to investigate the

influence of the treatment time, a 10 s treatment of the polymeric solution was performed. The resulting electrospun mat presented fibers having a large amount of beads (Fig. 2.27 B).

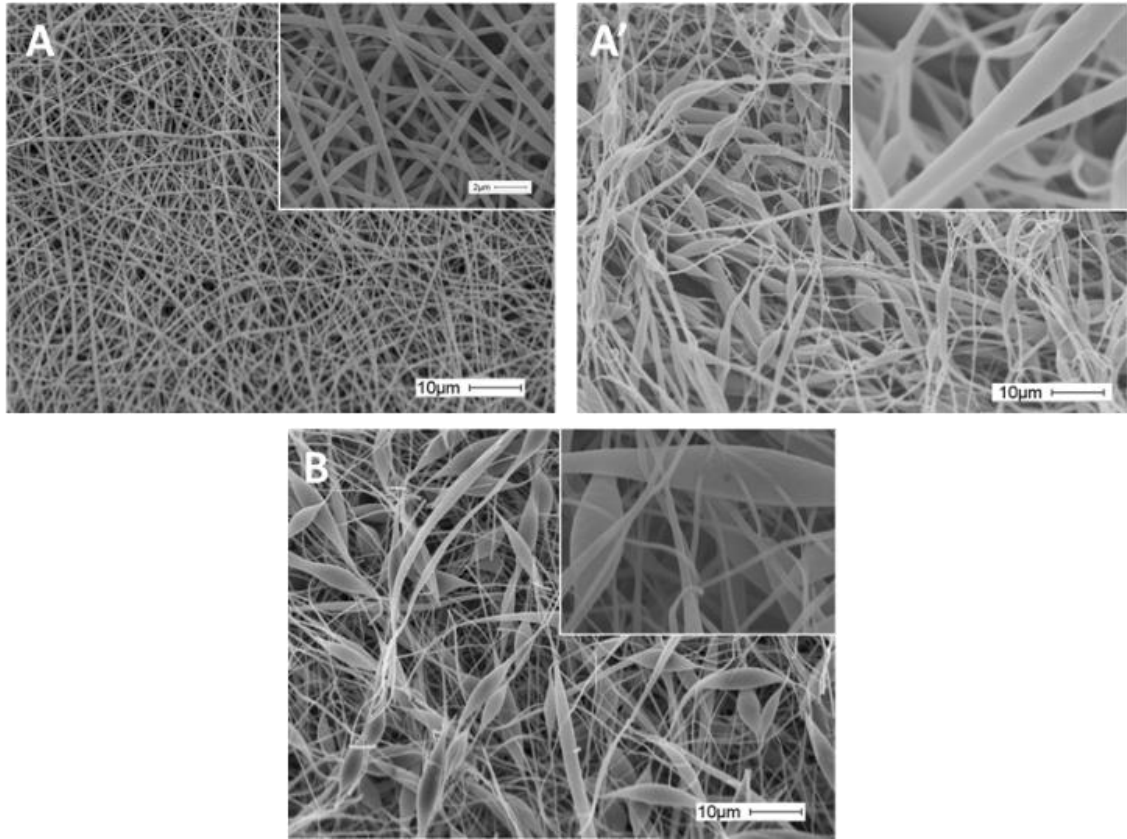


Fig. 2.27 PLLA fibers electrospun starting from a solution exposed to plasma jet driven by the nanopulsed generator. Mat resulting from electrospinning different polymeric solution treated for 120 seconds and sample collected at the beginning of the electrospinning process (A), solution treated for 120 seconds and collected 210 minutes after the beginning of the electrospinning process (A'), treated for 10 seconds and sample collected at the beginning of the electrospinning process (B) [57].

Good quality fibers without beads or defects could also be obtained electrospinning a solution exposed to the plasma jet driven by positive homopolar square wave for 2 min, as shown in Fig. 2.28 A. The persistence of the improvement of the electrospinnability persisted up to 120 minutes after plasma treatment (Fig. 2.28 A'). A

treatment time of 10 s (Fig. 2.28 B) does not allow the production of a good quality fiber membrane (Fig. 2.28 B).

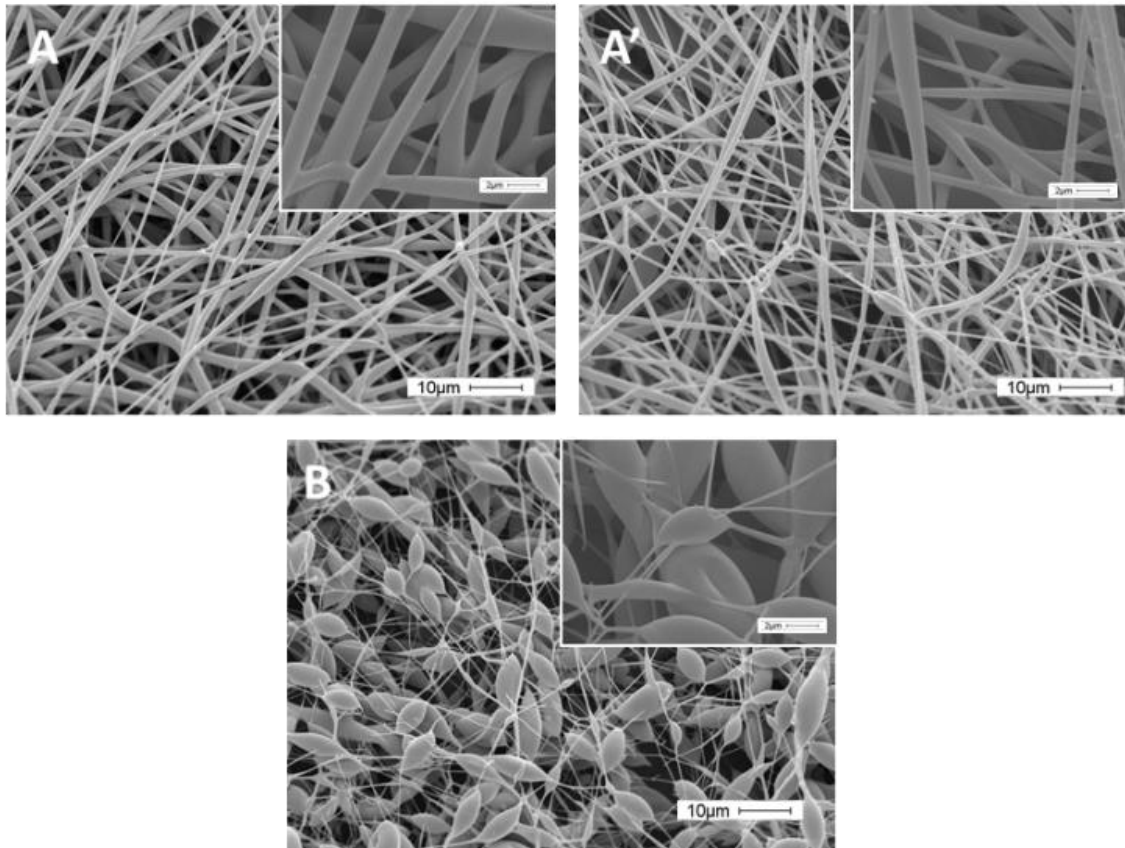


Fig. 2.28. PLLA fibers electrospun starting from a solution exposed to plasma jet driven by positive homopolar square wave. Mat resulting from electrospinning different polymeric solution treated for 120 seconds and sample collected at the beginning of the electrospinning process (A), solution treated for 120 seconds and collected 210 minutes after the beginning of the electrospinning process (A'), treated for 10 seconds and sample collected at the beginning of the electrospinning process (B) [57]

When the solution was treated with plasma driven by a non homopolar square wave at 40 kV Vpp, the electrospin of good PLLA fibers without defect occurred only within the first 30 minutes (Figure 2.29 A) after plasma exposure. Indeed after 60 minutes the presence of defects was found and is reported in Figure 2.27A'. On the

other hand, if the solution has been treated with a plasma driven by a non homopolar square at 20 kV Vpp (Figure 2.30 fibers presented defects along their axis also if the treated solution was electrospun immediately after the plasma treatment. The exposure of the polymeric solution to the plasma generated with a negative homopolar square wave induced many defects in the electrospun fibers (Figure 2.31).

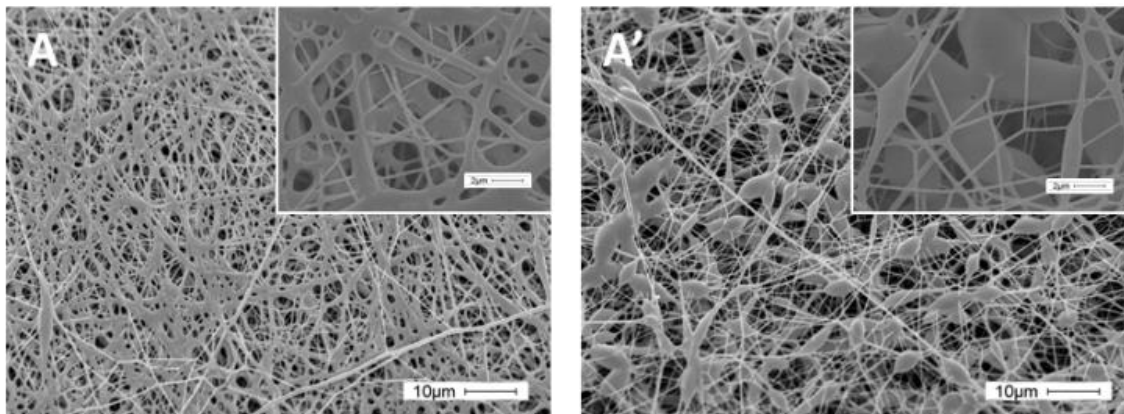


Figure 2.28. PLLA fibers electrospun started from a solution exposed to the plasma, driven by a non homopolar square wave at 40 kV Vpp. Solution treated for 120 seconds and collected at the beginning of the electrospinning process (A), solution treated for 120 seconds and sample collected 60 minutes after the beginning of the electrospinning process (A') [57]

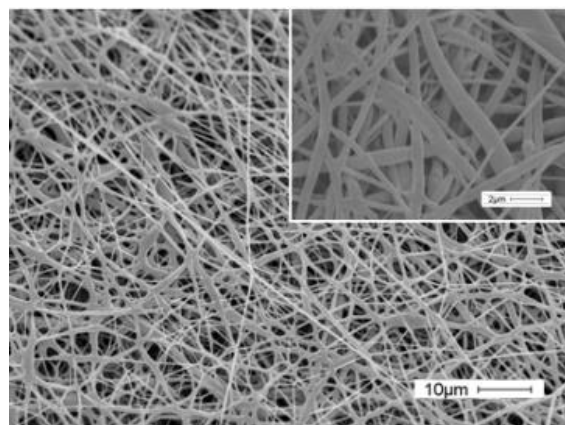


Fig. 2.29. PLLA fibers electrospun starting from a solution exposed to the plasma, driven by a non homopolar square wave at 20 kV Vpp. Solution treated for 120 seconds and collected immediately after the start of the electrospinning process [57]

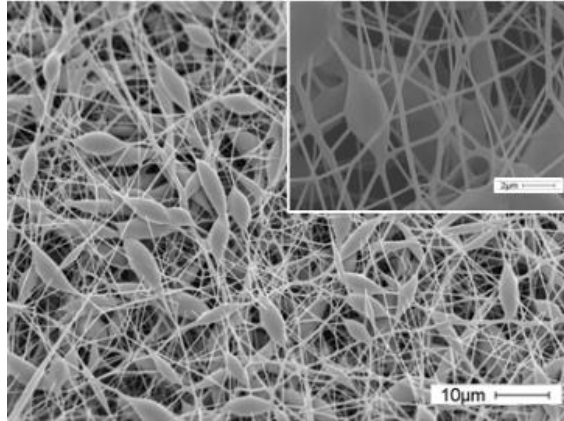


Fig. 2.30. PLLA fibers electrospun started from a solution exposed to the plasma, driven by a negative homopolar square wave. Solution treated for 120 seconds and collected immediately after the start of the electrospinning process [57]

Concerning the solutions treated with plasma driven by homopolar sinusoidal (Figure 2.32), triangular (Figure 2.33) and sawtooth (Figure 2.34) waveforms, all the resulting electrospun mats resulted made by fibers with defects. The first one had spun fibers with a little amount of defects, the second one a little bit more and the last one a large number of beads.

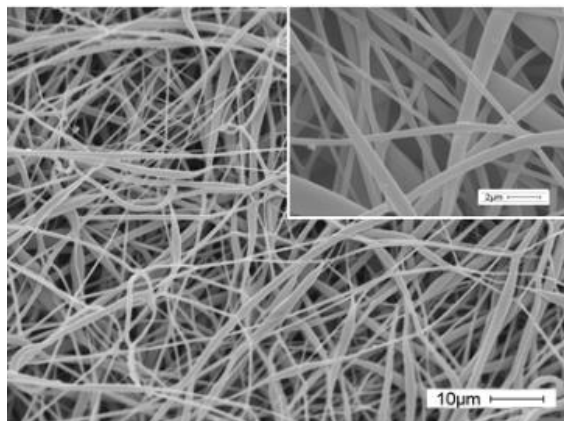


Fig. 2.32. PLLA fibers electrospun starting from a solution exposed to the plasma, driven by an homopolar sinusoidal wave. Solution treated for 120 seconds and collected at the beginning of the electrospinning process [57]

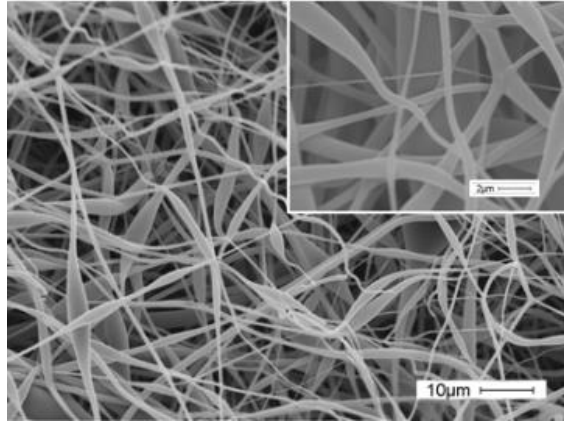


Fig. 2.33 PLLA fibers electrospun starting from a solution exposed to the plasma, driven by an homopolar triangular wave. Solution treated for 120 seconds and collected at the beginning of the electrospinning process [57]

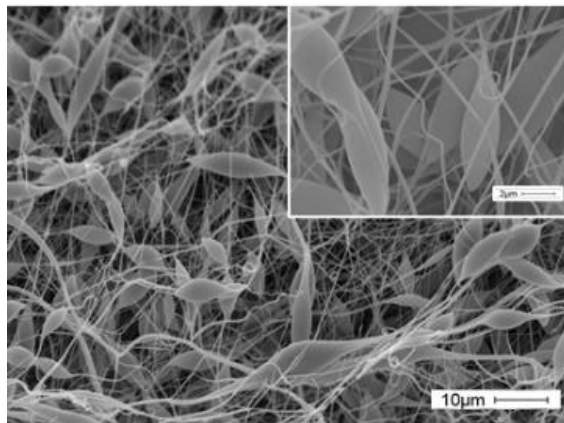


Fig. 2.34 PLLA fibers electrospun starting from a solution exposed to the plasma, driven by an homopolar sawtooth square wave. Solution treated for 120 seconds and collected at the beginning of the electrospinning process [57]

As reported before, the non homopolar sinusoidal and triangular waveforms (Figure 2.35 and 2.36) gave the worst results in terms of fiber morphology. Finally, among all cases the homopolar waveforms have shown better results compared to the non homopolar ones.

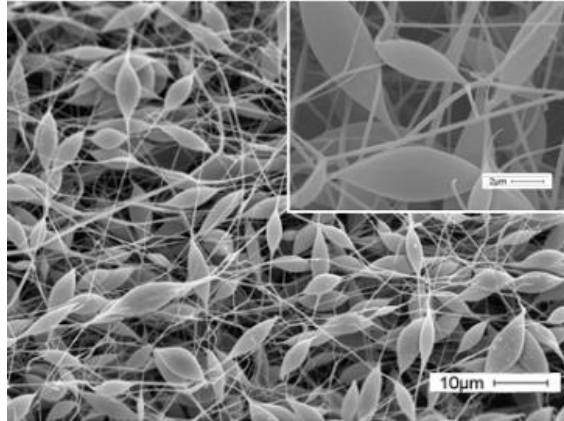


Fig. 2.35. PLLA fibers electrospun starting from a solution exposed to the plasma, driven by a non homopolar sinusoidal wave. Solution treated for 120 seconds and collected at the beginning of the electrospinning process [57]

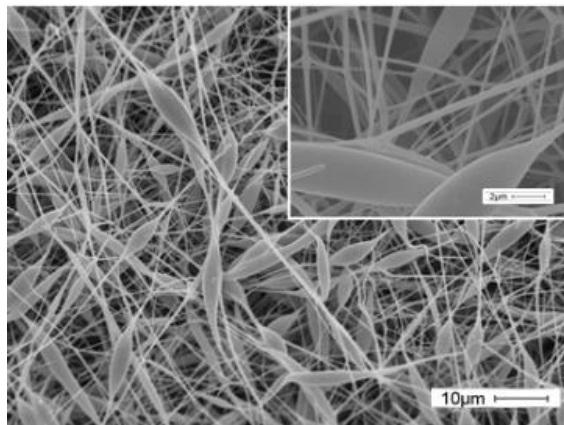


Fig. 2.36. PLLA fibers electrospun starting from a solution exposed to the plasma, driven by a non homopolar triangular wave. Solution treated for 120 seconds and collected at the beginning of the electrospinning process [57]

The fiber diameter distributions of mat consisting of defect free fibers were measured with the aim of verify the influence of the plasma treatment of the electrospinning solution on the fiber dimension of the resulting mat (Table 2). Fibers in the mat electrospun starting from a solution exposed to the plasma driven by nanopulsed waveform showed an average diameter of 390 nm, while the

electrospinning polymeric solution treated with the plasma jet driven by the homopolar square voltage produced a mat with a average fiber diameter of 1,49 μm .

Waveform shape	Fiber diameter [μm]
Nanopulsed	0.39 ± 0.14
Homopolar square	1.49 ± 0.44

Table 2. Fiber diameter distribution [36]

In conclusion, among the investigated plasma treatment, only a plasma treatment performed using the plasma jet driven by the nanopulsed waveform allows the production of nanofibrous mat made of defect free fibers.

An evaluation of the influence of the operative conditions of the nanosecond pulsed plasma jet on the improvement of the electrospinnability was also performed. The PLLA solutions in DCM were exposed to the plasma source under different operating conditions. In particular, plasma PV and PRF were varied, as well as treatment time (Δt). Moreover, the influence of the volume (vol) of treated solution was also evaluated. In fig. 2.37, SEM images of mat produced starting from different treated solutions are shown.

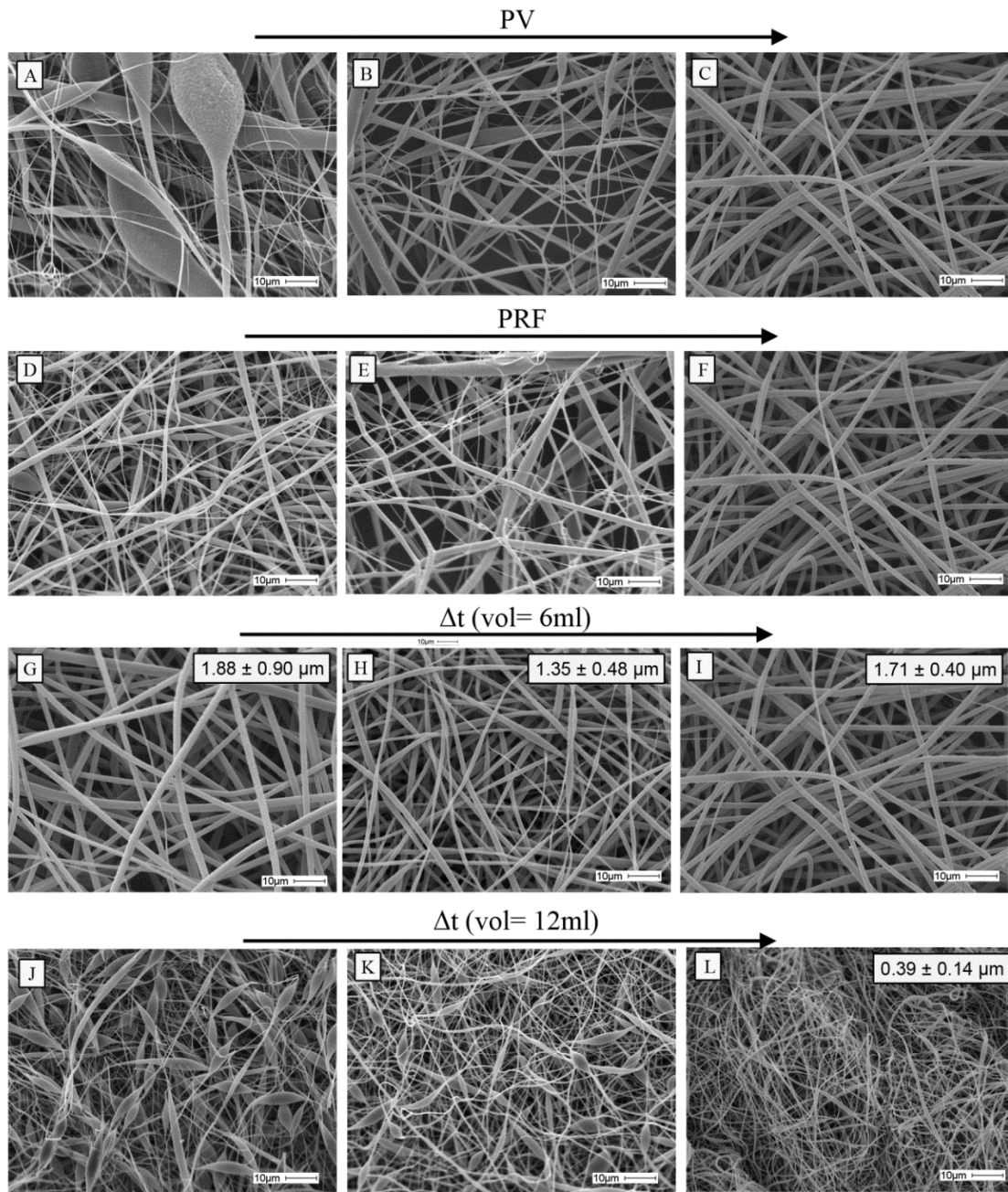


Fig. 2.37. SEM images of fibers obtained electrospinning solutions treated with plasma jet operated with an Ar flow rate of 2 slpm and a stand-off of 5 mm. First row: treated volume = 6 ml, PRF = 1000 Hz, treatment time = 120 s, PV = 17 kV (A), 22 kV (B), 27 kV (C). Second row: treated volume = 6 ml, PV = 27 kV, treatment time = 120 s, PRF = 500 Hz (D), 750 Hz (E), 1000 Hz (F). Third row: treated volume = 6 ml, PV = 27 kV, PRF = 1000 Hz, treatment time = 10 s (G), 30 s (H), 120 seconds (I). Fourth row: treated volume = 12 ml, PV = 27 kV, PRF = 1000 Hz, treatment time = 10 s (J), 30 s (K), 120 s (L). [36]

Overall, a decrease of beads number and a significant improvement of PLLA fiber morphology were found in the mat electrospun starting from the PLLA solution treated with the nanosecond plasma jet for all the investigated operating conditions adopted (compare Fig. 2.26 with Figure 2.37). In particular, Fig. 2.37A highlights that a plasma treatment (PV = 17 kV, PRF = 1000 Hz, treatment time = 120 s) of 6 ml of polymer solution did not completely prevent the formation of beads along the fibers (Figure 2.37A). Increasing the peak voltage up to 22 kV while keeping constant the other operating conditions (Figure 2.37B) resulted in a decrease of beads along the fibers; no beads can be observed when the electrospinning solution was treated using the plasma driven by a peak voltage set at 27 kV (Figure 2.37C). The influence of PRF is shown in Figure 2.37D-F, reporting SEM images of mats produced from a 6 ml plasma treated polymeric solution (PV = 27 kV, treatment time = 120 s); the increase of the PRF from 500 Hz (Figure 2.37D) to 750 Hz (Figure 2.37E) induced a decrease of defects along the fibers, which completely disappeared when the treatment was performed with PRF set at 1000 Hz. Since the best results in terms of fiber morphology of the electrospun mats were found if a plasma treatment with a peak voltage of 27 kV and a pulse repetition frequency of 1000 Hz was performed, this treatment was selected to investigate the effect of treatment time and treated volume on the improvement of the electrospinnability of the polymeric solution. It should be noticed that treating the polymeric solution with the same Ar jet without igniting the plasma discharge (Ar flow rate = 2 slpm, stand-off = 5 mm), resulted in a negligible improvement of fiber morphology with respect to the produced from an untreated solution ones.

With respect to the effect of the treatment time on fiber morphology, for a solution volume of 6 ml, 10 s of plasma treatment (PV = 27 kV, PRF = 1000 Hz) were sufficient to produce defect-free fibers showing micrometric diameter (Figure 2.37G); the increase of the duration of the plasma treatment to 30 s (Figure 2.37H) and 120 s (Figure 2.37I) did not induce further improvements of fiber morphology. If larger solution volume (12 ml) was treated, 10 s of plasma treatment (PV = 27 kV, PRF = 1000 Hz) allowed the production of mats with beaded fibers, as reported in (Figure 2.37J); increasing the treatment time to 30 s resulted in an improved fiber morphology (Figure 2.37K) but a plasma treatment of 120 s was indispensable for the production of totally defect-free fibers, as reported in Figure 2.37L. Moreover, fibers produced from a 12 ml solution display significantly smaller diameters ($0.39 \pm 0.14 \mu\text{m}$ for the case of PV = 27 kV, PRF = 1000 Hz, Ar flow rate = 2 slpm, stand-off = 5 mm, treatment time = 120 s, Figure 8L) with respect to those produced from a 6 ml solution ($1.71 \pm 0.40 \mu\text{m}$ for the same operating conditions, Figure 2.37I). To explain this result, measurements of the weight of the solutions before and after plasma treatment were performed to evaluate the solvent evaporation during the treatment and evaluate the consequent change of polymer concentration. Indeed, it is known that a strong dependence of fiber diameter on polymer concentration exists: higher polymer concentration in the electrospinning solution causes a higher fiber diameters in the electrospun mat [47, 58]. The plasma treatment of 6 ml of a 10 w/v% solution induced an increase in polymer concentration up to 13 w/v%, whereas the final concentration was 11 w/v% if the treated volume was equal to 12 ml. It is possible to conclude that the higher fiber diameter in the case of 6 ml solution with respect to 12 ml one might be ascribable to the increase of

polymer concentration in the plasma treated solutions. Interestingly, it is important to mark that if an untreated solution having a concentration 13 w/v% is electrospun, the final mats is made of non-homogeneous fibers with a large number of defects (Figure 2.26 A-C). To investigate if the increase of polymer concentration of 6 ml solution was induced by the plasma treatment, the change of polymer concentration due to the evaporation of DCM at RT by exposing the solution to open air for 120 s was calculate. It was found that the polymer concentration increased from 10 w/v% up to 10.2 w/v%. Therefore, we can speculate that the solvent evaporation, that is responsible of the remarkable increase of polymer concentration, could be due to the increase of solution temperature during plasma treatment. Indeed, the temperature of the plasma discharge, measured on the surface of the solution by means of the aforementioned fiber optic temperature sensor, was 33.1 ± 0.9 °C while RT was 26.5 ± 0.5 °C.

In order to evaluate the improvement of the electrospinnability of the plasma treated polymer solution during time, we measured the fibers average diameter of a mat electrospun starting from the same plasma treated polymeric solution at different delay time between plasma application and the electrospinning process (aging) (Fig.2.38). This analysis has been carried out using the following operating conditions: PV = 27 kV, PRF = 1000 Hz, Ar flow rate = 2 slpm, stand-off = 5 mm, treatment time = 120 s and polymer solution volume = 12 ml. As expected, the improvement of electrospinnability induced by plasma treatment is limited in time, i.e. up to 180 minutes (Figure 2.38A and 2.38B). On the contrary, after 210 minutes plasma effect decays, as demonstrated by the appearance of beads in the electrospun fibers).

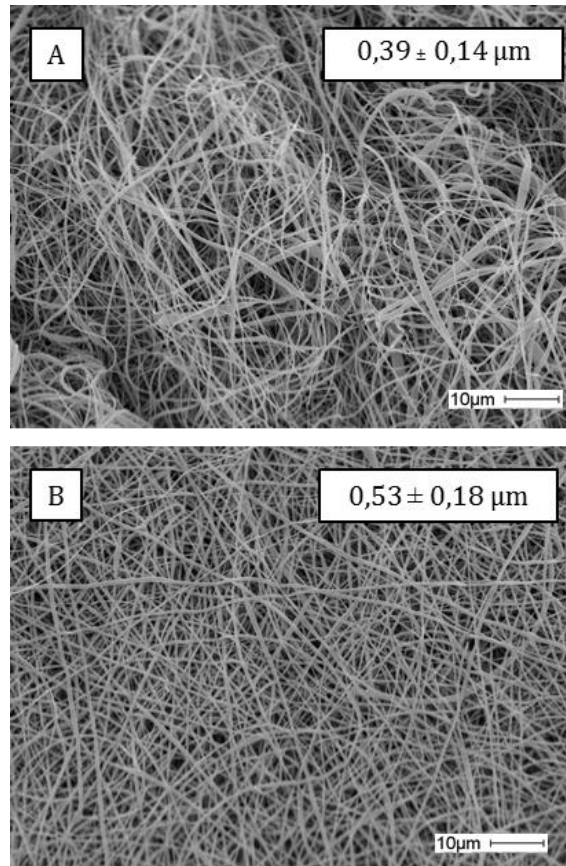


Fig. 2.38 SEM images of fibers obtained from plasma treated polymeric solutions. Treated volume = 12 ml, PV = 27 kV, PRF = 1000 Hz, Ar flow rate = 2 slpm, aging = 0 minutes (A), 180 minutes [36]

Shi et alii [49] demonstrated that, in the case of PEO water solution, the improvement of fiber morphology might be related to plasma generation of charged molecules which ionize polymer chains, modifying solution characteristics. Similarly, for PLLA solution in DCM we speculate that the presence of charges together with reactive species typically produced in an Ar plasma jet, such as hydroxyl radicals (OH) and nitrogen based species [59,60], might affect the solution electrospinnability by three factor:

1) increasing solution conductivity,

- 2) increasing chain hydrodynamic volume in case of acquisition of a net charge by the polymeric chains,
- 3) creating species that favour interactions among macromolecular chains.

The presence of reactive species in the discharge adopted in the experiments was attested in the analysis of the OES spectra shown in the previous chapter. Overall, OH radicals, excited N_2 and N_2^+ were detected in the discharge, in agreement with literature results [38, 54, 59, 60].

The hypothesized role of charged and reactive species on the modification of solution properties could also explain the improvement of electrospinnability if the plasma jet is driven by higher PRF and PV; indeed, these two electrical parameters are well known to modify the plasma jet characteristics: their increase results in a higher concentration of charged and reactive species [61, 62] as well as in an elongation of the plasma plume in open air [63]. On the other hand, high treatment times required to increase electrospinnability of large solution volumes may be necessary to ensure the production and diffusion of enough plasma generated reactive species. Finally, the ageing of the plasma treated polymer solution, resulting in a progressive decrease of electrospinnability, can be probably appointed to the progressive recombination of the reactive and charged species introduced in the solution during its interaction with the jet plume. However, further investigations and characterizations are required to elucidate the mechanism by which plasma acts in improving solution spinnability. Focusing on the electrospinning process, we observed a macroscopic change of the electrospinning jet path for a plasma treated solution. In particular, the elongation of the jet straight segment and the development of whipping instability, that are two of

the four stages that characterize the electrospinning process - as modeled by Reneker and co-workers [64] – dramatically changed. Indeed, a more extended whipping instability was observed after plasma exposure, evidence of strong changes occurring in polymer solution as a consequence of plasma treatment [36].

REFERENCES

- [1] Ehlbeck J, Schnabel U, Polak M, Winter J, von Woedtke Th, Brandenburg R, von dem Hagen T and Weltmann K-D 2011 *J. Phys. D: Appl. Phys* 44 013002
- [2] Leipold F, Kusano Y, Hansen F and Jacobsen T 2010 *Food Control* 21 1194–8
- [3] Fernández A, Noriega E and Thompson A 2013 *Food Microbiol* 33(1) 24-9
- [4] Xu G, Zhang G, Shi X, Ma Y, Wang N and Li Y 2009 *Plasma Sci. Technol.* 11 84–8
- [5] Morfill G E, Shimizu T, Steffes B and Schmidt H U 2009 *New J. Phys.* 11 115019
- [6] Fridman G, Peddinghaus M, Ayan H, Fridman A, Balasubramanian M, Gutsol A, Brooks A and Friedman G 2006 *Plasma Chem. Plasma Process.* 26 425–442
- [7] Fridman G, Friedman G, Gutsol A, Shekhter A B, Vasilets V N and Fridman A 2008 *Plasma Process. Polym.* 5 000–000
- [8] Kim G C, Lee H J and Shon C H 2009 *J. Kor. Phy. Soc.* 54(2) 628-632
- [9] Kim C H, Bahn J H, Lee S H, Kim G Y, Jun S I, Lee K and Baek S J 2010 *J. Biotech.* 150 530-8
- [10] Keidar M, Walk R, Shashurin A, Srinivasan P, Sandler A, Dasgupta S, Ravi R, Guerrero-Preston R and Trink B 2011 *Brit. J. Canc.* 105 1295-1301
- [11] Kurita H, Nakajima T, Yasuda H, Takashima K, Mizuno A, Wilson J I B and Cunningham S 2011 *Appl. Phys. Lett.* 99 191504
- [12] Yan X, Xiong Y, Zou F, Zhao S, Lu X, Yang G, He G and Ostrikov K 2012 *Plasma Process. Polym.* 9(1) 59-66
- [13] Huang J, Li H, Chen W, Lv G H, Wang X Q, Zhang G P, Ostrikov K, Wang P Y and Yang S Z 2011 *Appl. Phys. Lett.* 99 253701

- [14] Joh H M, Kim S J, Chung T H and Leem S H 2012 *Appl. Phys. Lett.* 101 053703
- [15] Volotskova O, Hawley TS, Stepp M A and Keidar M. 2012 *Sci. Rep.* 2 636-645
- [16] Kolb J F, Mattson A M, Edelblute C M, Hao X, Malik M A and Heller L C 2012 *IEEE Trans. Plasma Sci.* 40(11) 3007-3026
- [17] Jijie R, Luca C, Pohoata V and Topala I 2012 *IEEE Trans. Plasma Sci.* 40(11) 2980-5
- [18] Zhao S, Xiong Z, Mao X, Lu X, He G, Han F and Yang G 2012 *IEE Trans. Plasma Sci.* 40(9) 2179-2184
- [19] Weltmann K D, Kindel E, Brandenburg R, Meyer C, Bussiahn R, Wilke C and von Woedtke T 2009 *Contrib. Plasma Phys.* 49(9) 631-640
- [20] O'Neill F T, Twomey B, Law V J, Milosavljevic V, Kong M, Anghel S D, and Dowling D 2012 *IEEE Trans. Plasma Sci.* 40(11) 2994-3002
- [21] Deng X L, Nikiforov A Y, Vanraes P and Leys C 2013 *J. Appl. Phys.* 113 023305
- [22] Xiong Q, Nikiforov A Y, Li L, Vanraes P, Britun N, Snyders R, Lu X P and Leys C 2012 *Eur. Phys. J. D* 66 281
- [23] Hong Y, Lu N, Pan J, Li J, Wu Y and Shang K F 2013 *J. Electrostatics* 71 93
- [24] van Gessel A F H, Hrycak B, Jasinski M, Mizeraczyk J, van der Mullen J J A M and Bruggeman P J 2013 *J. Phys. D: Appl. Phys.* 46 095201
- [25] Xiong Q, Nikiforov A Y, Gonzalez M A, Leys C and Lu X P 2013 *Plasma Sources Sci. Technol.* 22 015011
- [26] Shao T, Long K, Zhang C, Yan P and Zhang S (2008) *J. Phys. D: Appl. Phys.* 41:215203
- [27] Ayan H, Fridman G, Gutsol A F, Vasilets V N, Fridman A and Friedman G 2008) *IEEE Trans. Plasma Sci.* 36:504-8
- [28] Oh J S, Olabanji O T, Hale C, Mariani R, Kontis K and Bradley J W 2011 *J. Phys. D: Appl.*

Phys. 44:155206

- [29] Dobrynin D, Fridman G, Friedman G and Fridman A 2009 *New J. Phys.* 11 115020
- [30] Nastuta A V, Topala I, Grigoras C, Pohoata V and Popa G 2011 *J. Phys. D: Appl. Phys.* 44 105204
- [31] Kalghatgi S U, Fridman G, Cooper M, Nagaraj G, Peddinghaus M, Balasubramanian M, Vasilets V N, Gutsol A F, Fridman A and Friedman G 2007 *IEEE Trans. Plasma. Sci.* 35 (5) 1559-1566
- [32] Heinlin J, Morfill G, Landthaler M, Stolz W, Isbary G, Zimmermann J L, Shimizu T and Karrer S 2010 *JDDG* 8 1–9
- [33] Wertheimer M R, Saoudi B, Ahlawat M and Kashyap R 2012 *Plasma Process. Polym.* 9 (10) 955-967
- [34] Knoerzer K, Murphy A B, Fresewinkel M, Sanguansri P and Coventry J 2012 *Inn. Food Sci. Emerg. Technol.* 15 23-30
- [35] Lu X, Laroussi M, Puech V 2012 *Plasma Sources Sci. Technol.* 21:034005
- [36] Colombo V, Fabiani D, Focarete M L, Gherardi M, Gualandi C, Laurita R, Zaccaria M 2014 *Plasma Process. Polym.* DOI: 10.1002/ppap.201300141
- [37] Boselli M, Colombo V, Ghedini E, Gherardi M, Laurita R, Liguori A, Sanibondi P, Stancampiano A, 2014 *Plasma Chem. and Plasma Process.* 1-17
- [38] M. Boselli, V. Colombo, M. Gherardi, R. Laurita, A. Liguori, P. Sanibondi, A. Stancampiano, 2015 *IEEE Trans. Plasma Sci., Special issue on Atmospheric Pressure Plasma Jets and their Applications* DOI: 10.1109/TPS.2014.2381854
- [39] Ungate C D, Harleman D R, Jirka G H 1975 Stability and mixing of submerged turbulent jets at low Reynolds numbers, MIT Energy Lab.

- [40] Folletto M, Douat C, Fontane J, Joly L, Pitchford L, Puech V 2013 *Proceedings of 31th International Conference on Phenomena in Ionized Gases - ICPIG, 14-19 Jul 2013, Granada, Spain*
- [41] *An introduction to Electrospinning and nanofibers*, S. Ramakrishna, K. Fujihara, W.E. Teo, T.C. Lim & Z. Ma, 2005 *World Scientific Publishing Co. Pte. Ltd, NJ, USA*
- [42] N. Bhardwaj, S. C. Kundu, 2010 *Biotechnology Advances* 28 325–347
- [43] C. Kriegel, A. Arrechi, K. Kit, D. J. McClements, J. Weiss, 2008 *Critical Reviews in Food Science and Nutrition*, 48 775–797
- [44] H. Fong, D.H. Reneker, 1999 *Polymer*, 40, 4585
- [45] X. Geng, O-H. Kwon, J. Jang, 2005 *Biomaterials* 26 5427-5432
- [46] Cn-M. Hsu, S. Shivkumar, 2004 *Macromol. Mat. Eng.* 289 334-340
- [47] Z-M. Huang, Y-Z. Zhang, M. Kotaki, S. Ramakrishna, 2003 *Comp. Sc. Technol.* 63 2223-2253
- [48] Y.-F. Goh, I. Shakir, R. Hussain, 2013 *J. Mater. Sci.* 48, 3027–3054
- [49] Q. Shi, N. Vitichuli, M. McCord, J. Nowak, M. Bourham, Z. Lin, X. Zhang, B. Guo, 2010 *Journal of Polymer Science* 49 115–122
- [50] P. Bruggeman, C. Leys, 2009 *J. Phys. D: Appl. Phys.* 42 053001
- [51] Y. Lu, S. F. Xu, X. X. Zhong, K. Ostrikov, U. Cvelbar, D. Mariotti, 2013 *EPL* 102 15002
- [52] Q. Shi, N. Vitichuli, J. Nowak, J. M. Caldwell, F. Breidt, M. Bourham, X. Zhang, M. McCord, 2011 *Eur. Polym. J.* 47(7) 1402-1409
- [53] A. Descoedres, Ch. Hollenstein, G. Walder, R. Demellayer, R. Perez, 2008 *Plasma Sources Sci. Technol.* 17 024008

- [54] M. Boselli, V. Colombo, E. Ghedini, M. Gherardi, R. Laurita, A. Liguori, P. Sanibondi, A. Stancampiano, *Characterization of a plasma jet for biomedical applications: composition, temperature, fluid dynamics and plasma structure*, proceedings of 21th ISPC, Cairns, Australia, August 2013
- [55] S-H. Tan, R. Inai, M. Kotaki, S. Ramakrishna, 2005 *Polymer* 46 6128-6134
- [56] F. Yang, R. Murugan, S. Wang, S. Ramakrishn, 2005 *Biomaterials* 26 2603-2610
- [57] Colombo V, Fabiani D, Focarete ML, Ghedini E, Gherardi M, Gualandi C, Laurita R, Sanibondi P, Zaccaria M, *Solid Dielectrics (ICSD), 2013 IEEE International Conference on (pp. 358-361) Bologna*
- [58] S. L. Shenoy, W. D. Bates, H. L. Frisch, G. E. Wnek, 2005 *Polymer* 46 3372-3384
- [59] A. F. H. van Gessel, K. M. J. Alards and P. J. Bruggeman, 2013 *J. Phys. D: Appl. Phys.* 46 265202
- [60] A. V. Pipa , S. Reuter , R. Foest and K.-D. Weltmann, 2012 *J. Phys. D: Appl. Phys.* 45 085201
- [61] Q. Li, H. Takana, Y. K. Pu, H. Nishiyama, 2012 *Appl. Phys. Lett.* 100 133501
- [62] N. Georgescu, C. P. Lungu, A. R. Lupu, M. Osiac, 2010 *IEEE Trans. Plasma Sci.* 38 (11) 3156-3162
- [63] Q. Xiong, X. Lu, K. Ostrikov, Z. Xiong, Y. Xian, F. Zhou, C. Zou, J. Hu, W. Gong, Z. Jiang, 2009 *Physics of Plasmas* 16 043505
- [26], D. H. Reneker, A. L. Yarin, E. Zussman, S. Koombhongse, W. Kataphinan. 2006 *Polymeric Nanofibers, ACS Symposium Series Oxford University Press*, p. 7-20

4. Acknowledgments

The results reported in Chapter 2.3 have been published in <http://dx.doi.org/10.1002/ppap.201300141> © 2014 1999-2015 John Wiley & Sons, Inc and <http://dx.doi.org/10.1109/ICSD.2013.6619847> © 2013 IEEE
The results reported in Chapter 2.2 have been published in <http://dx.doi.org/10.1007/s11090-014-9537-1> © 2014 Springer International Publishing AG and <http://dx.doi.org/10.1109/TPS.2014.2381854> © 2015 IEEE

In reference to John Wiley & Sons, Inc, IEEE and Springer International Publishing AG copyrighted material which is used with permission in this thesis, John Wiley & Sons, Inc, IEEE and Springer International Publishing AG does not endorse any of University of Bologna's products or services.

The whole is other than the sum of the parts.

I am part of a strange family, without their support I could not be able to complete this long journey. Thank you for your love.

I am part of an extraordinary research group. In primis, I want to thank Prof. Vittorio Colombo, for his teachings, in science and in life. My gratitude goes also to Matteo, for all the time he spent with me discussing about science and life. A special thanks to Anna, Augusto, Daniela, Marco, Emanuele and Enrico, for all the time spent in the laboratory together.

I am part of a huge network of research groups. Thanks to the staff of the other groups I have met in these years and I have had the opportunity to work with, especially Prof. Peter Lukes, Prof. Davide Fabiani, Prof. Maria Letizia Focarete, Dr. Chiara Gualandi and Dr. Marco Zaccaria.

I am part of a fantastic group of friend. Thank you for your help in these years.

Thank you whole, I am part of you.